Engineering dipolar quantum matter via inter-layer interactions

A Thesis

submitted to
Indian Institute of Science Education and Research Pune
in partial fulfillment of the requirements for the
BS-MS Dual Degree Programme

by

Pranay Nayak

Indian Institute of Science Education and Research Pune
Dr. Homi Bhabha Road,
Pashan, Pune 411008, INDIA.

June, 2021

Supervisor: Dr. Rejish Nath

Certificate

This is to certify that this dissertation entitled Engineering dipolar quantum matter via inter-layer interactions towards the partial fulfilment of the BS-MS dual degree programme at the Indian Institute of Science Education and Research, Pune represents study/work carried out by Pranay Nayak at Indian Institute of Science Education and Research under the supervision of Dr. Rejish Nath, Associate Professor, Department of Physics , during the academic year 2020-2021.

Dr. Rejish Nath

Committee:

Dr. Rejish Nath

Prof. M.S. Santhanam

This thesis is dedicated to all my loved ones

Declaration

I hereby declare that the matter embodied in the report entitled Engineering dipolar quantum matter via inter-layer interactions are the results of the work carried out by me at the Department of Physics, Indian Institute of Science Education and Research, Pune, under the supervision of Dr. Rejish Nath and the same has not been submitted elsewhere for any other degree.

Pranay Nayak

Acknowledgments

During these testing times, studying and doing science with peace of mind cannot take for granted. I found myself perturbed on many occasions. Some of my colleagues had it worse. Numerous people provided me with care and displayed tremendous amounts of patience. They may not have directly helped me with my thesis work, but it has been just as important, if not more. To all of them, my gratitude is sincere.

I thank Dr. Rejish Nath for all the care and guidance he gave me throughout my stay with his group. He has always been there, be it physics, life, or everything in between. His advice has helped me understand the ways of science research and allowed me to take a few steps further as the scientist I want to be.

I want to extend my thanks to all the faculty at IISER Pune's various departments. You showed care and love for us when we were away from home. I thank Prof. M. S. Santhanam for agreeing to be my Expert. I also thank Dr. Sachin Jain for his constant display of enthusiasm towards Physics. I am forever grateful to all faculties from the HSS and Biology departments who helped me understand the meaning of science and its place in society. The academic resources provided by IISER have been of immense help to me. The INSPIRE scholarship by DST, Bharat Sarkar, has supported me as a BS-MS student. My gratitude is with the people in science, who take it upon themselves and make science education accessible through lectures, seminars, talks, etc., on the internet.

I thank all the group members, especially Rathejit, Gautam, Dr. Chinmayee Mishra, and Swarnavo, for all the discussions we had in group meetings and otherwise. My time at IISER during my 5th year was made bright by the *Lime Juice gang*. Some friends were not on campus but provided much-needed support from the rears. Lastly, but most importantly, my family has always been there and always will be. Thank You!

Abstract

This thesis discusses how inter-layer dipole-dipole interactions (DDIs) introduce structural modifications in dipolar Bose-Einstein condensates (DBECs). We demonstrate this in a bi-layer system with three DBECs. We also discuss how this model can be extended to create a periodic 1D lattice. We have two or more trapped condensates in one layer, whereas in the second layer, we have an untrapped cigar-shaped one. With a proper choice of dipole orientations, the inter-layer DDIs effectively form a trapping potential for the condensate in the second layer, with non-trivial patterns in the potential landscape. The latter results in a non-trivial stable density pattern in the condensate in the second layer, offering a unique scenario of engineering a quantum matter in hand. We demonstrate control over the density profile and coherence of the matter-wave peaks. The technique we use here may also be helpful for the controlled generation of exotic states imitating supersolids - a long-sought-after state of matter with both crystal and superfluid character.

Contents

Introduction

The quantum world is subversive to our notions in daily life. Engineering the states of physical systems obeying quantum principles is at the heart of fundamental and applied sciences. Many emerging fields such as quantum computation and quantum simulation rely solely on this, as first suggested by Feynman in 1959 [1]. Semi-conductors, lasers, interferometers, atomic clocks, etc., are outstanding achievements due to this quest. Therefore, engineering quantum states or matter waves is at the heart of quantum technological applications. Currently, there are many synthetic quantum systems available in labs around the world. Among them, Bose-Einstein condensates (BECs) have their special place due to the enormous studies that have been conducted with them, which enlarged our horizon of fundamental problems which we could address.

One of the most significant advantages of an ultracold atom system like BEC is that it is highly controllable. We can engineer them into different geometries, particularly quasi-one-dimensional cigar or quasi-two-dimensional disk-shaped condensates. The latter is done by modifying the trapping frequencies of the external harmonic potentials. In addition, we can control the inter-particle interactions, which is at the heart of quantum simulation of exotic quantum many-body phases. In the most common setups of alkali atoms, the interaction between the particles is short-range and isotropic, typically modeled by a delta-function potential. The interaction strengths are governed by a single parameter called the s-wave scattering length. The interactions can be made attractive or repulsive, or even non-interacting through Feshbach resonances, driven by either magnetic or optical fields.

Condensation of highly magnetic atoms such as Erbium, chromium, and Dysprosium opened up a novel class of condensates called the dipolar BECs. The dipole-dipole interactions are both anisotropic and long-range in nature, introducing qualitatively new features in the BEC-Physics [2, 3]. These can be traced to the emergence of roton-like excitations

in the Bogoliubov spectrum [4] and the observation of quantum droplets and supersolids over the last few years [5, 6]. The dipolar potential is also highly tunable utilizing rotating electric or magnetic fields [7]. The long-range nature of dipolar potential leads to inter-layer effects in completely disconnected condensates. In general, the inter-layer effects are less explored in dipolar condensates. The studies have shown that inter-layer interaction may have significant consequences in the physics of dipolar condensates. For instance, the Bogoliubov spectrum of disconnected condensates exhibits collective modes shared among condensates, which leads to soliton crystals/filamentation, soliton molecules, etc.

In this thesis, by exploiting the inter-layer dipole-dipole interaction, we show that a matter-wave can be engineered in a highly controlled manner. In particular, our studies reveal highly complex and intriguing structures in the dipolar condensates in their ground state. We also show that interlayer interactions can confine condensates in the absence of external fields and induce density modulated condensates resembling the exotic supersolids. We believe that our studies will have far-reaching consequences in the field of quantum technologies and the fundamental understanding of matter waves.

The structure of this thesis is as follows:

- **Chapter 1:** We start with the general definition of Bose-Einstein condensation. Introduce the concept of off-diagonal long-range order (ODLRO) and explain the physical meaning of the order parameter of the condensation in case of weakly interacting Bose gases. The mean-field description of the BEC via Gross-Pitaevskii equation (GPE) and the concepts of reducing effective dimensions of the condensates along with solitons are briefly mentioned towards the end of this chapter.

- **Chapter 2:** Aim of this chapter is to narrow down the focus to dipolar interactions in BEC. We discuss the GPE for Dipolar BECs and emphasize the novelty of the anisotropic and long-range character of the interaction. We talk about the unique instabilities like phonon and roton-maxon, which hint towards the rich physics of dipolar interactions. We finish the chapter with a glance at some novel phenomena studied in Dipolar BECs and the possibility to engineer BECs via interactions between isolated condensates, owing to the long-range nature of dipolar interactions.

- **Chapter 3:** This chapter introduces our system of study in detail. We derive the 3D and Quasi-1D GPEs which govern the evolution and ground state of the system.

Further, we obtain a variational solution to our problem using a Gaussian ansatz. The stability of the solutions is also discussed using the soliton criteria. It is in this chapter that we demonstrate a scheme to entrap a Q-1D condensate just via inter-layer interactions.

- **Chapter 4:** In the final chapter of the thesis, we establish that we can obtain a stable Quasi-1D Dipolar BEC using inter-layer interactions. We propose a technique that harnesses inter-layer dipolar interactions to entrap a stable BEC and induce controllable non-trivial structures in the ground state. This is achieved in a Q-1D condensate without any external layers. Verification with 3D simulations is made, and the coherence between the peaks in the non-trivial structures is controlled.

Achievement of entrapment and non-trivial structure in a matter-wave without the aid of external lasers opens new avenues in BEC experiments. Harnessing inter-layer interactions to engineer quantum matter may light a path of possibilities in quantum information endeavors.

Chapter 1

The Bose-Einstein Condensate

Attempts towards explaining the nature of cold have been made since time immemorial. However, modern scientific investigations are believed to have started with Robert Boyle (1627 - 91), regarded as one of the founders of Modern Chemistry and the experimental scientific method. He systematically debunked the ancient beliefs and laid forward the modern understanding of cold. Later, Physicists discovered the vast expanse between the lowest temperatures accessible to them and the lowest possible limit known to them. With the vast unknown came a race to liquefy gases. In 1898, James Dewar liquefied Hydrogen at 23K. His contemporary, Heike Kamerlingh Onnes, went further and liquefied Helium at 4K in 1908. This feat led to a Nobel Prize in 1913 [8] and to the mind-boggling phenomenon of superfluidity and superconductivity. This fascinating nature of matter at ultracold temperatures wrecked the minds of Physicists for the next century and led to countless revolutions in our understanding of nature.

1.1 Inception

In 1925, Albert Einstein predicted Bose-Einstein Condensation by applying Bose statistics for photons onto massive non-interacting particles. This seemingly impractical idea, however, was resurrected to explain superfluidity. After 70 years of scientific advancement, Bose-Einstein Condensate (BEC) was finally demonstrated in 1995 [9] by Ketterle's group. In the meantime, heavyweights like Feynman, Landau, Onsager, Penrose, Bogoliubov, and many

others developed the microscopic theories, excitation spectrum, condensate fraction, and vital concepts like Off-diagonal long-range order to explain BEC and superfluid [10–12]. We will now proceed to have a look at those.

1.2 Ideal Bose Gas

In 1924, Satyendra Nath Bose proposed a new way of explaining photons and blackbody radiation in his letter to Albert Einstein. He obtained Plank's Law for Blackbody radiation using nothing but his proposed statistics, without making any reference to classical laws. Einstein took it a step further and proposed a similar statistic, now known as Bose statistics, for counting massive particles.

$$\langle n \rangle = f\left(\epsilon_p\right) = \frac{1}{e^{\frac{\epsilon-\mu}{k_B T}}-1} \tag{1.1}$$

Here, he realised that for an ideal non-interacting Bose gas, there seemed to be a singularity in density of states. To see how, recall

$$n = \frac{N}{V} = \frac{1}{V}\sum_{\epsilon} f(\epsilon) = \int_0^\infty d\epsilon f(\epsilon) g(\epsilon) \tag{1.2}$$

where, $g(\epsilon)$ is density of states. For a smooth distribution, one gets

$$n = \frac{1}{4\pi^2}\left(\frac{2m}{\hbar^2}\right)^{\frac{3}{2}} \int_0^\infty d\epsilon \frac{\sqrt{\epsilon}}{e^{\frac{\epsilon-\mu}{k_B T}}-1}. \tag{1.3}$$

We have equation 1.1 for a grand canonical ensemble, and one can have any arbitrarily large number for n in a given volume. From equation 1.3 this demands arbitrarily large values of μ. But, chemical potential in Bose systems in equilibrium has an upper bound, that is the ground state energy - a conundrum. To solve this, we go back a step and express the density of states as a discrete sum over the momentum states. Here we had converted the $\sum_k$ to $\int_k$ and ignored that we cannot do so when $k_B T$ is of the order of μ. To remedy, we count for the ground state occupation separately $n = n_0 + n_{k\neq 0}$ - where, n_0 is the density of zero momentum state and $n_{k\neq 0}$ can be approximated by equation 1.3.

Essentially, from 1.3 we get $\mu(T, n)$ and for fixed n, we find a $T = T_c > 0$ such that μ approaches its upper limit. After, this temperature is reached, lowering it further makes particles occupy the ground state in larger, macroscopic quantities. This is called Bose-Einstein Condensation. We shall introduce the formal definition to this phase transition later in this chapter.

1.2.1 Off-diagonal long-range order (ODLRO)

This section and the following deal with a Bose system without any assumptions on the exact nature of their interactions unless stated otherwise. The phenomenon of Off-diagonal long-range order (ODLRO) is a defining feature of Bose Condensation. To demonstrate it, we can start with the one-body density matrix in second quantized notation.

$$n^{(1)}\left(\mathbf{r}, \mathbf{r}'\right) \equiv \mathrm{Tr}\left\{\hat{\rho}\hat{\psi}^{\dagger}(\mathbf{r})\hat{\psi}\left(\mathbf{r}'\right)\right\} \equiv \left\langle\hat{\psi}^{\dagger}(\mathbf{r})\hat{\psi}\left(\mathbf{r}'\right)\right\rangle \tag{1.4}$$

where, $\hat{\rho}$ is the density matrix, $\hat{\psi}^{\dagger}(\mathbf{r})$ and $\hat{\psi}\left(\mathbf{r}'\right)$ are bosonic creation and annihilation operators respectively in position basis. If a many body system occupies a pure state described by a N-body wavefunction $\Psi_n\left(\boldsymbol{r}_1, \boldsymbol{r}_2, \ldots, \boldsymbol{r}_N\right)$, one can write the one-body density matrix as

$$n_n^{(1)}\left(\boldsymbol{r}, \boldsymbol{r}'\right) = N \int \mathrm{d}\boldsymbol{r}_2 \cdots \mathrm{d}\boldsymbol{r}_N \Psi_n^*\left(\boldsymbol{r}, \boldsymbol{r}_2, \ldots, \boldsymbol{r}_N\right) \Psi_n\left(\boldsymbol{r}', \boldsymbol{r}_2, \ldots, \boldsymbol{r}_N\right), \tag{1.5}$$

where we do $N-1$ integrals. For indistinguishable particles, this implies that one can interpret $n_n^{(1)}\left(\boldsymbol{r}, \boldsymbol{r}'\right)$ as the probability amplitude to annihilate a particle at $\mathbf{r}'$ and create it at $\mathbf{r}$ without perturbing the given quantum state. Here, we can get a sneak-peek at ODLRO. When a system undergoes Bose condensation, the de-Broglie wavelengths of the particles overlap and all particles become indistinguishable. So, even at large separations, $\mathrm{s} = |\mathbf{r} - \mathbf{r}'|$, we get a finite probability to annihilate a particle at $\mathbf{r}'$ and create it at $\mathbf{r}$ without perturbing the given quantum state. Thus, $n_n^{(1)}\left(\boldsymbol{r}, \boldsymbol{r}'\right)$ does not vanish even at large separations.

For a thermal ensemble one can easily extend equation 1.5 as

$$n^{(1)}\left(\boldsymbol{r}, \boldsymbol{r}'\right) = \frac{1}{Z} \sum_n \mathrm{e}^{-E_n/kT} n_n^{(1)}\left(\boldsymbol{r}, \boldsymbol{r}'\right), \tag{1.6}$$

where $Z = \sum_n \mathrm{e}^{-E_n/kT}$ is the partition function. If the system is uniform and isotropic, in the thermodynamic limit we have

$$n^{(1)}(\boldsymbol{r}, \boldsymbol{r}') = n^{(1)}(s) = \frac{1}{V} \int \mathrm{d}\boldsymbol{p} n(\boldsymbol{p}) \mathrm{e}^{-\mathrm{i}\boldsymbol{p}\cdot\boldsymbol{s}/\hbar}. \tag{1.7}$$

If the distribution over momentum $\mathbf{p}$ was well-behaved, as it is for bosons at large temperatures, $\lim_{s\to\infty} n^{(1)}(s) = 0$. But, when the temperature is low enough for the ground state to get populated and the system has a well-defined chemical potential as a function of temperature and N, we have a singularity

$$n(\boldsymbol{p}) = N_0 \delta(\boldsymbol{p}) + \tilde{n}(\boldsymbol{p}). \tag{1.8}$$

One thus finds, as predicted by Landau, Lifshitz, Penrose and Onsager (1951 - 1956) that

$$n^{(1)}(s)_{s\to\infty} \to n_0, \tag{1.9}$$

where $n_0 = N/V$. This is called off-diagonal long-range order. This is a mathematically elegant and general version of what we did in previous section to deal with the problem of adding more particles to the system.

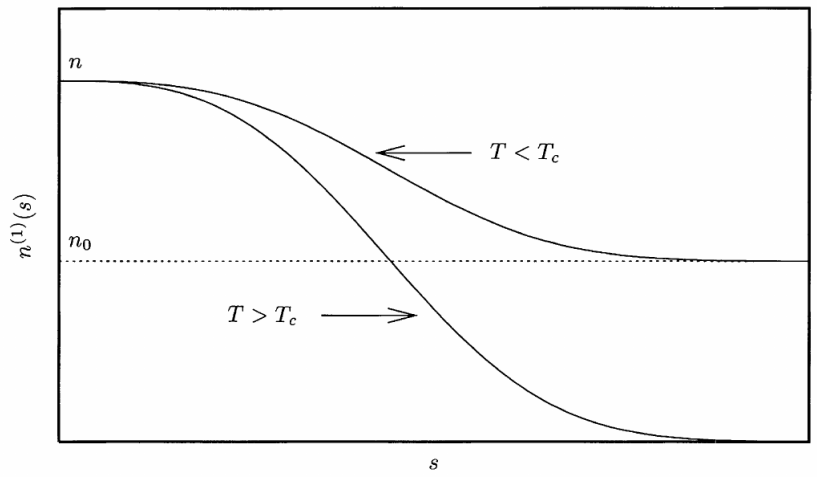

Figure 1.1: Off-diagonal one body density as a function of s = $|\mathbf{r}-\mathbf{r}'|$ for a weakly interacting dilute Bose gas.
Figure Courtesy: [11]

1.2.2 Order parameter

Let us consider the eigenfunctions $\varphi_i(\boldsymbol{r})$, and eigenvalues n_i of the one-body density matrix $n^{(1)}(\boldsymbol{r}, \boldsymbol{r}')$.

$$\int \mathrm{d}\boldsymbol{r}' n^{(1)}(\boldsymbol{r}, \boldsymbol{r}')\, \varphi_i(\boldsymbol{r}') = n_i \varphi_i(\boldsymbol{r}). \tag{1.10}$$

We now have a natural orthonormalized basis to expand the one body density matrix as

$$n^{(1)}(\boldsymbol{r}, \boldsymbol{r}') = \Sigma_i n_i \varphi_i^*(\boldsymbol{r}) \varphi_i(\boldsymbol{r}') = N_0 \varphi_0^*(\boldsymbol{r}) \varphi_0(\boldsymbol{r}') + \sum_{i \neq 0} n_i \varphi_i^*(\boldsymbol{r}) \varphi_i(\boldsymbol{r}'). \tag{1.11}$$

Here n_i tells us the occupation of the single particle wave-functions ϕ_i. Bose Condensation is macroscopic occupation of a single-particle state, say $i = 0$ (i.e. $N_0/N = O(1)$). Consider separating the annihilation field operator as follows:

$$\hat{\Psi}(r) = \varphi_0(r)\hat{a}_0 + \sum_{i \neq 0} \varphi_i(r)\hat{a}_i \tag{1.12}$$

Here we introduce the Bogoliubov approximation by replacing $\hat{a}_0$ with a c-number $\sqrt{N_0}$. This is justified in the limit of macroscopic occupation when $N_0 >> 1$. Now, the errors due to ignoring the commutation relations (and thus reducing status of $\hat{a}_0$ from an operator to a c-number) are of $O(1)$, compared to the leading terms of $O(N)$. We thus rewrite the field annihilation operator as $\hat{\Psi}(\boldsymbol{r}) = \Psi_0(\boldsymbol{r}) + \delta\hat{\Psi}(\boldsymbol{r})$, where $\Psi_0 = \sqrt{N_0}\varphi_0$ and $\delta\hat{\Psi} = \sum_{i \neq 0} \varphi_i a_i$. The classical field operator Ψ_0 dubs as the condensate order parameter. Its value is zero for temperatures above the critical temperature, and is otherwise a complex function with a pre-factor of $O(\sqrt{N})$. As one can notice from equation 1.11, the order parameter is defined upto a phase only. There is a gauge freedom in choosing the phase of Ψ_0. This continuous symmetry is broken spontaneously when the system undergoes Bose condensation. Also, $\hat{a}_0 = const$ implies that the condensates with N_0 or $N_0 \pm 1$ have same physical properties, if all other quantum numbers remain the same. In fact, defining $\Psi_0 \equiv \langle N|\hat{\Psi}|N+1\rangle$ one can show that

$$\Psi_0(\boldsymbol{r}, t) = \Psi_0(\boldsymbol{r}) \mathrm{e}^{-\mathrm{i}\mu t/\hbar}, \tag{1.13}$$

where $\mu = E(N) - E(N-1) \sim \partial E/\partial N$ is the chemical potential, when average is taken over stationary states.

1.3 Weakly interacting Bose gases

Interactions play an essential role in the physics of dilute BEC. Usually one finds themselves tackling interaction by assuming a very dilute gas and reducing all effects of interactions to a delta potential in position space, usually dubbed as contact interaction.

$$V_{\text{contact}}(r) = \frac{4\pi\hbar^2 a}{m}\delta(r) \equiv g\delta(r) \tag{1.14}$$

The diluteness allows for assuming all interactions as two-body scatterings, dominated by the s-wave scattering length, a. One usually has a very high degree of control over the value of $'a'$, through Feshback Resonance [7]. These are responsible for the superfluid character of the BEC. In this section, we particularly explore the physics of dilute, weakly interacting Bose gas. We shall demonstrate the ODLRO and calculate the order parameter for such systems.

1.3.1 Bogoliubov Hamiltonian

The microscopic Hamiltonian of a Bose gas with only two-body interaction terms, in terms of field operators is:

$$\hat{H} = \int \left(\frac{\hbar^2}{2m}\nabla\hat{\Psi}^\dagger\nabla\hat{\Psi}\right)\mathrm{d}r + \frac{1}{2}\int \hat{\Psi}^\dagger\hat{\Psi}^{\dagger\prime}V(r'-r)\,\hat{\Psi}\hat{\Psi}'\mathrm{d}\boldsymbol{r}'\mathrm{d}\boldsymbol{r} \tag{1.15}$$

Clearly, we have assumed a specific form of interaction term but in the case of rarefied gases, this is very suitable. Now, we would consider $V(r'-r) = V_{contact}(r'-r)$ as in 1.15. In Fourier space, this becomes

$$\hat{H} = \sum \frac{p^2}{2m}\hat{a}^\dagger_{\boldsymbol{p}}\hat{a}_{\boldsymbol{p}} + \frac{g}{2V}\sum \hat{a}^\dagger_{\boldsymbol{p}_1+\boldsymbol{q}}\hat{a}^\dagger_{\boldsymbol{p}_2-\boldsymbol{q}}\hat{a}_{\boldsymbol{p}_1}\hat{a}_{\boldsymbol{p}_2}, \tag{1.16}$$

where $\hat{\Psi}(\boldsymbol{r}) = \sum_{\boldsymbol{p}}\hat{a}_{\boldsymbol{p}}1/\sqrt{V}\mathrm{e}^{\mathrm{i}p\cdot\boldsymbol{r}/\hbar}$.

Now one proceeds to do the Bogoliubov approximation in section 1.2.2 and expand the Hamiltonian 1.16 in decreasing orders of N, i.e. starting from $O(N^2)$ to $O(N)$. Then one can use the so-called Bogoliubov transformation to diagonalize the approximate Hamiltonian

and obtain the phonon excitation spectra and thus calculate partition function of the system. We will skip on the detailed calculation and show the resultant Hamiltonian.

$$\hat{H} = E_0 + \sum \epsilon(p)\hat{b}_p^\dagger \hat{b}_p \tag{1.17}$$

where the ground state energy, as obtained by Lee and Yang (1957) [13],

$$E_0 = g\frac{N^2}{2V}\left[1 + \frac{128}{15\sqrt{\pi}}\left(na^3\right)^{1/2}\right] \tag{1.18}$$

and the excitation spectra, also known as Bogoliubov spectra is,

$$\epsilon(p) = \left[\frac{gn}{m}p^2 + \left(\frac{p^2}{2m}\right)^2\right]^{1/2} \tag{1.19}$$

A very important point to emphasize here would be notice that at $p \to 0$, $\epsilon(p) \propto p$ i.e. a phonon spectrum and at large p we have free particle spectra. Recalling Landau's criteria for superfluids, one notices that $g \neq 0$ is what allows weakly interacting BEC to be a superfluid. A non-interacting BEC is not a superfluid.

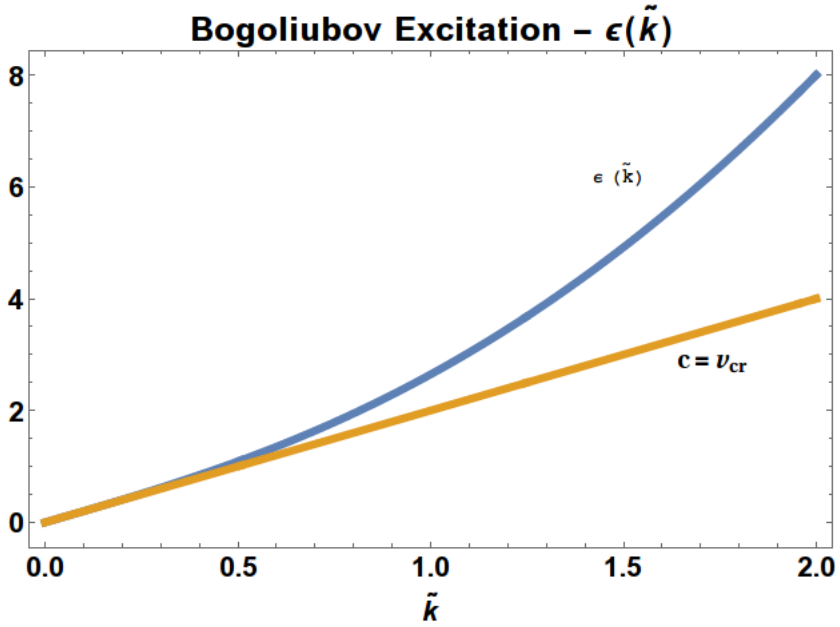

Figure 1.2: We have dimensionless bogoliubov excitation energy $\epsilon(\tilde{k})$ as a function of dimensionless wave-number $\tilde{k}$. One can see the v_{cr} in Landau's superfluid criteria is simply the speed of sound $c\ \alpha\ \sqrt{g}$ in weakly interacting Bose gases

1.4 Gross-Pitaevskii Equation (GPE)

We had defined the classical field $\Psi_0(\boldsymbol{r}, t)$ as the order parameter for our system describing BEC. Till now we have studied it for uniform systems, now we wish extend it to the case for non-uniform dilute Bose gases. To study dynamics of Ψ_0 we recall the following equation for evolution of an operator in Heisenberg picture:

$$\mathrm{i}\hbar\frac{\partial}{\partial t}\hat{\Psi}(\boldsymbol{r},t) = [\hat{\Psi}(\boldsymbol{r},t), \hat{H}] = \Bigg[-\frac{\hbar^2\boldsymbol{\nabla}^2}{2m} + V_{\text{ext}}(\boldsymbol{r},t) + \int \hat{\Psi}^\dagger(\boldsymbol{r}',t)\, V(\boldsymbol{r}'-\boldsymbol{r})\, \hat{\Psi}(\boldsymbol{r}',t)\, \mathrm{d}\boldsymbol{r}'\Bigg] \hat{\Psi}(\boldsymbol{r},t). \quad (1.20)$$

This is true for any general two-body potential. We then replace the quantum operator $\hat{\Psi}_0$ with the classical field $\Psi_0$to obtain the GPE in context of the weakly interacting case.

$$\mathrm{i}\hbar\frac{\partial}{\partial t}\Psi_0(\boldsymbol{r},t) = \left(-\frac{\hbar^2\boldsymbol{\nabla}^2}{2m} + V_{\text{ext}}(\boldsymbol{r},t) + g\left|\Psi_0(\boldsymbol{r},t)\right|^2\right)\Psi_0(\boldsymbol{r},t) \quad (1.21)$$

Equation 1.21 was obtained independently by Gross and Pitaevskii in 1961. This non-linear equation finds analogy in non-linear optics. Equation 1.21 is valid only for large N dilute systems, much below the critical temperature for Bose-Einstein Condensation. Here, we can comfortably ignore the thermal and quantum depletion and substitute the classical field for the quantum operator. Also, since we totally ignored the exact form of inter-species potential and simply broke it into a dipolar and a contact part - obtained from scattering, we can only probe physics at scales larger than scattering length 'a' or dipolar length $a_{\text{dd}} \equiv C_{\text{dd}}m/(12\pi\hbar^2)$. Also, in the same limit, we can obtain the number density of the condensate

$$n(\boldsymbol{r}) = \left|\Psi_0(\boldsymbol{r})\right|^2. \quad (1.22)$$

Equation 1.22 is the reason why the order parameter is often called the wave-function of the condensate. Even though, its technically not, as we'll see. Recalling equation 1.13 for stationary states, we find that GPE has a time independent form

$$\left(-\frac{\hbar^2\boldsymbol{\nabla}^2}{2m} + V_{\text{ext}}(\boldsymbol{r}) - \mu + g\left|\Psi_0(\boldsymbol{r})\right|^2\right)\Psi_0(\boldsymbol{r}) = 0. \quad (1.23)$$

Strictly speaking, $\Psi_0(\boldsymbol{r})$ is not the condensate wavefunction, but the order parameter only. However, it plays a similar role and if often called a wavefunction. Having a look at the non-

linear equation 1.23, one wonders over the point that different values of chemical potential μ, won't give different orthogonal Ψ_0 as the equation is non-linear. The wavefunction can be obtained from the order parameter easily if one ignores any correlations between particles and thus assumes total independence in the probability distribution to write

$$\Phi_a\left(\boldsymbol{r}_1, \boldsymbol{r}_2, \ldots, \boldsymbol{r}_N\right) = \left(\frac{1}{\sqrt{N}}\Psi_a\left(\boldsymbol{r}_1\right)\right)\left(\frac{1}{\sqrt{N}}\Psi_a\left(\boldsymbol{r}_2\right)\right)\cdots\left(\frac{1}{\sqrt{N}}\Psi_a\left(\boldsymbol{r}_N\right)\right) \tag{1.24}$$

for the many-body wavefunction given a μ_a. Different Φ_a are orthogonal for different values of μ_a in the large N limit, as then, the product in equation 1.24 gives, $(\Phi_a, \Phi_b) = \left(N^{-1}\int \mathrm{d}\boldsymbol{r}\Psi_a^*\Psi_b\right)^N$ which goes to 0 since the term in brackets is always less than one. The claim that time independent GPE, equation 1.23 gives the the ground state of a system of dilute Bose gas with contact interactions has been rigorously proven [14].

1.4.1 Energy and momentum

The Energy, following 1.20 and applying Bogoliubov approximation, is

$$E = \int\left[\frac{\hbar^2}{2m}|\nabla\Psi_0|^2 + V|\Psi_0|^2 + \frac{g}{2}|\Psi_0|^4\right]\mathrm{d}^3\mathbf{r} = E_{\mathrm{kin}} + E_{\mathrm{pot}} + E_{\mathrm{int}}. \tag{1.25}$$

The terms give us the expression for Kinetic, potential and interaction energy for weakly interacting gas. For a time independent potential, E is conserved during a condensate's unitary evolution. The momentum is given as

$$\mathcal{P} = \frac{i\hbar}{2}\int\left(\Psi_0\nabla\Psi_0^* - \Psi_0^*\nabla\Psi_0\right)\mathrm{d}^3\mathbf{r}. \tag{1.26}$$

1.4.2 Condensates of reduced dimensionality

Here we will approximate the condensate dynamics with reduced dimensions. Details on criteria and the procedure are given in Appendix B and [15]. A brief explanation follows. Consider the external potential $V = 1/2(\omega_x^2x^2 + \omega_y^2y^2 + \omega_z^2z^2)$. The shape of a condensate of weakly interacting gas can be manipulated using the anisotropy of the Harmonic trap. For example, $\omega_x, \omega_y >> \omega_z$ gives a condensate shaped like a cigar along z. While, $\omega_x, \omega_y << \omega_z$ gives a flat pancake in $x - y$ plane.

Figure 1.3: Figure (a) is a cigar ($\omega_x, \omega_y >> \omega_z$) and (b) is the pancake ($\omega_x, \omega_y << \omega_z$).

In making these traps more anisotropic, we can reduce the dynamics of the system to one or two dimensions. Consider the prolate cigar for example. If the trap is tight enough in the x and y directions, we won't have to worry about dynamics in the radial plane. As, the relevant condensate dynamics will be of lower order in magnitude and one can approximate the condensate wave-function to break into independent parts:

$$\psi(x, y, z, t) = \psi_z(z, t) G_x(x) G_y(y) \tag{1.27}$$

where, G_x and G_y are Simple Harmonic Oscillator (SHO) ground states. More precisely, this is valid when $\mu_{1D} << \hbar \left(\omega_x \omega_y\right)^{1/2}$. Following that, we obtain the Quasi-1D GPE:

$$\mu_{1\mathrm{D}} \psi_z = -\frac{\hbar^2}{2m} \frac{\mathrm{d}^2 \psi_z}{\mathrm{d}z^2} + g_{1\mathrm{D}} \left|\psi_z\right|^2 \psi_z + \frac{1}{2} m \omega_z^2 z^2 \psi_z \tag{1.28}$$

where, the new parameters are defined as

$$g_{1\mathrm{D}} = \frac{g}{2\pi \ell_x \ell_y}, \quad \mu_{1\mathrm{D}} = \mu - \frac{\hbar \omega_x}{2} - \frac{\hbar \omega_y}{2} \tag{1.29}$$

Similarly for a very strong trap in z direction, one will get a flat pancake shaped condensate and the equations for $\psi_\perp(x, y, t)$, which is defined by the approximation, $\psi(x, y, z, t) = \psi_\perp(x, y, t) G_z(z)$, are as follows:

$$\begin{aligned} \mu_{2\mathrm{D}} \psi_\perp &= -\frac{\hbar^2}{2m} \left(\frac{\mathrm{d}^2 \psi_\perp}{\mathrm{d}x^2} + \frac{\mathrm{d}^2 \psi_\perp}{\mathrm{d}y^2} \right) + g_{2\mathrm{D}} \left|\psi_\perp\right|^2 \psi_\perp + \frac{1}{2} m \left(\omega_x^2 x^2 + \omega_y^2 y^2\right) \psi_\perp, \\ g_{2\mathrm{D}} &= \frac{g}{\sqrt{2\pi} \ell_z}, \quad \mu_{2\mathrm{D}} = \mu - \frac{\hbar \omega_z}{2} \end{aligned} \tag{1.30}$$

This way for cigar shape or pancake shaped condensates, we can often do analysis and description in reduced dimensions.

1.5 Solitons

In this section, we work in Quasi-1D regime with no trap in longitudinal direction (here x) , using time dependent form of 1.28.

$$i\hbar\frac{\partial\psi}{\partial t} = -\frac{\hbar^2}{2m}\frac{\partial^2\psi}{\partial x^2} + g|\psi|^2\psi \tag{1.31}$$

This differential equation is extremely well studied in non-linear optics and is known to be integrable. For instance, norm of ψ, momentum P and Energy E are all conserved. This equation also supports self bound solutions known as *solitons* [16, 17]. Their defining properties are:

1. The form is permanent and unchanging.
2. The profile is localized in space.
3. Upon collision with other solitons, they come out unaltered.

This makes them analogous to particles. In case of weakly interacting Bose gases, system can support two types of solitons, depending on the sign of interaction - dark solitons for $g > 0$ and bright solitons for $g < 0$.
A note of caution, 1.28 and the one above are just approximations to a full 3-D system. In reality, these are just approximate solitons.

Dark Solitons

These are supported in the regime $g > 0$. They are localised density minimas with a phase jump across them. The general form of this excited state of condensate is

$$\psi(x,t) = \sqrt{n_0}\left\{B\tanh\left[\frac{B(x-ut)}{\xi}\right] + i\frac{u}{c}\right\}\exp\left(-\frac{i\mu t}{\hbar}\right), \tag{1.32}$$

where, $0 < u \leq c$ - speed of sound in the condensate is the propagation velocity of soliton. A review on dark solitons in condensates can be found here [18]. At $u = 0$, one obtains a stationary black soliton with π phase jump. For the other extreme $u = c$, one obtains a soliton which is indistinguishable from the uniform background. A dark soliton is a 1-D phase defect.

Dark solitons in condensates were first experimentally reported in [19, 20]. However, a relatively long-living (a few seconds) soliton was reported in [21] where the condensate was in Q-1D regime and the Q-1D GPE was verified. These solitons were formed by changing phase of condensate along the longitudinal axis by making one part and shining laser on other to change phase of that part. These phase jump created dark solitons which evaporated in time due to thermal interactions. When the condensate is not narrow enough, the dark soliton *stripe* bends and gives rise to what is known as *snake instability*, which later on give rise to quantized vortices [22, 23].

Bright Soliton

These are supported in the regime $g < 0$ when attractive interactions overcome the dispersion. They are localised density maximas which form the ground state in a regime where uniform condensates are unstable. The single bright soliton, moving at speed $0 < u \leq c$, has order parameter

$$\psi(x,t) = \sqrt{\frac{1}{2\xi_s}}\,\mathrm{sech}\left(\frac{x-ut}{\xi_s}\right)\exp[if(x,t)+i\phi] \tag{1.33}$$

where $\xi_s = 2\hbar^2/m|g|$ and

$$f(x,t) = \frac{mux}{\hbar} - \frac{t}{\hbar}\left(\frac{mu^2}{2} - \frac{\hbar^2}{2m\xi_s^2}\right) \tag{1.34}$$

is the phase factor. Unlike dark solitons, the density and speed of propagation of a bright soliton are decoupled. A review on bright solitons could be found in [24]. Bright solitons in real condensate are unstable. The attractive interaction allows for condensates to get narrower and narrower until they collapse to a singularity. One can show this by using a Gaussian variation ansatz and calculating a minima for energy. The procedure to do that will be shown soon. Experimentally they were first reported in [25, 26] and in more recent times, their collision properties against one another and against potentials was demonstrated in [27, 28].

Chapter 2

Dipolar Bose Gases

As we have mentioned in the previous chapter, interactions play a huge role in the physics of Bose-Einstein Condensates. Simply changing signs of the weakly interacting delta potential 1.15 via Feshbach resonance changes the physics upside down in the context of solitons. Adding and tuning in various exotic interactions might give us unexpected results or some exotic physics to admire and subsequently exploit. Talking about interactions of long-range and anisotropic nature might appear a new world of phenomena before us. And it sure does, as we will see in this chapter. Now we will have a look at the physics of Bose-Einstein condensation with long-range and anisotropic dipolar interactions.

2.1 Dipolar interactions

Throughout the thesis, we will consider polarized dipoles. That is, all dipoles in the sample would be pointing in the same direction. The interaction potential then goes as:

$$V_{\mathrm{dd}}(r) = \frac{C_{\mathrm{dd}}}{4\pi}\frac{1-3\cos^2\theta}{r^3}. \tag{2.1}$$

where, θ is the angle between polarization direction and relative vector between the particles $\mathbf{r}$, and $C_{dd} = \mu_0\mu^2$, μ being the permanent dipole moment of the species and μ_0, the permeability of free space. Condensation of ^{52}Cr, with magnetic moment of 6.0 Bohr magneton was achieved way back in 2004 [29]. Focus on Dipolar interactions has been substantial [2, 3],

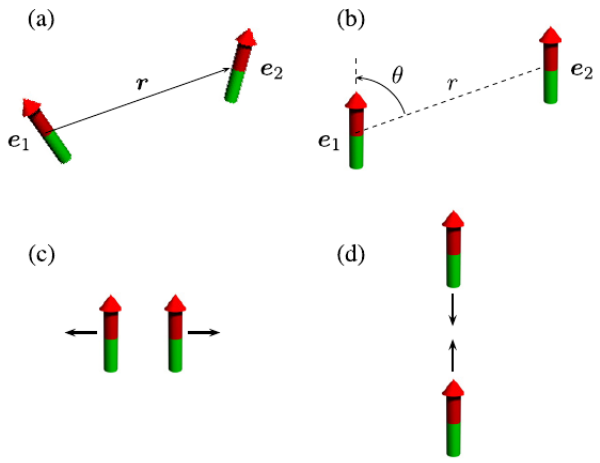

Figure 2.1: In this thesis, we only consider the polarised case (b), (a) is unpolarised and not considered. The anisotropy can be seen in (c) and (d) where orientation determines whether they repel or attract respectively.
Figure Courtesy: *The Physics of Dipolar Bose Gas by Lahaye et. al. [2]*

after the advent of promising cooling and trapping techniques for Polar molecules [30, 31]. In 2009, people at JILA were able to create ultracold gas of rubidium–potassium molecules in their ground rotovibrational state [32] and similar work was done for LiC molecules [33]. Further, species with electric dipole moment as well as magnetic dipole moment are also predicted to show interesting physics [34]. These achievements allow us to expect BEC in strong dipolar regimes. Even with a Cr BEC which has a small magnetic moment of $6\mu_B$ [29], one could get very interesting physics. Rydberg atoms have shown immense potential as candidates to quantum computer and quantum simulators [35].

2.2 GPE for Dipolar Bose Gas

Again, we replace the quantum operator $\hat{\Psi}_0$ with the classical field Ψ_0 in equation 1.20 and obtain the GPE for $V(\mathbf{r}-\mathbf{r}')$ sum of dipole 2.1 and contact potential 1.15.

$$\mathrm{i}\hbar\frac{\partial}{\partial t}\Psi_0(\boldsymbol{r},t)=\left(-\frac{\hbar^2\boldsymbol{\nabla}^2}{2m}+V_{\mathrm{ext}}(\boldsymbol{r},t)+g\left|\Psi_0(\boldsymbol{r},t)\right|^2+\int\left|\Psi_0\left(\boldsymbol{r}',t\right)\right|^2V_{\mathrm{dd}}\left(\boldsymbol{r}-\boldsymbol{r}'\right)\mathrm{d}^3r'\right)\Psi_0(\boldsymbol{r},t) \tag{2.2}$$

Again, we can only probe physics at scales larger than scattering length 'a' or dipolar length $a_{\mathrm{dd}}\equiv C_{\mathrm{dd}}m/(12\pi\hbar^2)$. Unlike for weakly interacting Bose gas with 1.15 potential, there is no

mathematically rigourous proof that 2.3 gives the ground state.
Time independent for of GPE is

$$\left(-\frac{\hbar^2\boldsymbol{\nabla}^2}{2m}+V_{\text{ext}}(\boldsymbol{r})-\mu+g\left|\Psi_0(\boldsymbol{r})\right|^2+\phi_{dd}(\mathbf{r})\right)\Psi_0(\boldsymbol{r})=0 \tag{2.3}$$

where, $\phi_{dd}(\mathbf{r})$ is the dipolar term in equation 1.21.

2.2.1 Bogoliubov excitations - Soliton Instability

To calculate the Bogoliubov excitations from the GPE, we can do the following. One adds perturbations to the wavefunction $\psi=\sqrt{n}+u(\mathbf{r})e^{i\omega_k t}+v^*(\mathbf{r})e^{-i\omega_k t}$ where, $u(r)$, $v^*(r)$ are complex plane wave excitation [36] and n is density of the perturbed ground state solution. For, uniform condensate, n is a constant and one obtains the following dispersion relation

$$\epsilon(k)=\sqrt{\frac{\hbar^2k^2}{2m}\left[\frac{\hbar^2k^2}{2m}+2n\left(g+\frac{4\pi g_d}{3}\left(3\cos^2\theta-1\right)\right)\right]}. \tag{2.4}$$

where, θ is angle between polarisation axis and momentum vector $\mathbf{k}$. For $g_d=0$ one gets back the Bogoliubov dispersion relation for contact potential only. In large k limit, we get the free particle dispersion relation $\epsilon(k)\approx\frac{\hbar^2k^2}{2m}$. Depending on values of g and g_d one can get imaginary values of excitation energy. This indicates presence of instability in the system. For $k\to 0$, $g_d=0$ and $g<0$ we find that the uniform condensate has instability, as seen in the section on bright solitons. Although these *phonon instability* results are for uniform condensates, they make good approximation in trapped case if the excitation wavelengths are small enough and condensate doesn't change much in density in the neighbourhood.
In case for dipolar gases, as seen in Cr BEC under soliton instability [37], the collapse reveals the anisotropy of Dipolar interactions.

2.2.2 Roton-Maxon instability

In 2003, existence of roton-maxon spectra in the excitation of DBECs was demonstrated by Santos et. al. [38]. Since then the physics of DBECs has enriched further and further. Unlike in ^4He,here one can soften the roton mode, i.e. lower the minima close to zero even in

weakly interacting regime, thus giving theoretical tractability. Achievement of roton mode population has been made [4]. This has motivated search for supersolid states of matter - self-organised density modulations on top of a superfluid flow. It should be noted that most such studies also deal with beyond mean-field corrections, dubbed LHY, while calculating the ground state [39]. It basically accounts for quantum fluctuations ignored in our mean-field treatment 1.21.

Consider a Dipolar Bose gas in pancake shaped trap. All the dipoles are pointing up and as you keep increasing g_d the repulsion increases. However, there comes a point when repulsion is so strong that the dipoles tend to get on top of each other and despite the Q-2D geometry, feel the 3D effect of dipolar potential. Tuning the values of g and g_d one can induce what is known as *roton instability*, first discussed in [40]. For, a 2D condensate, similar to as

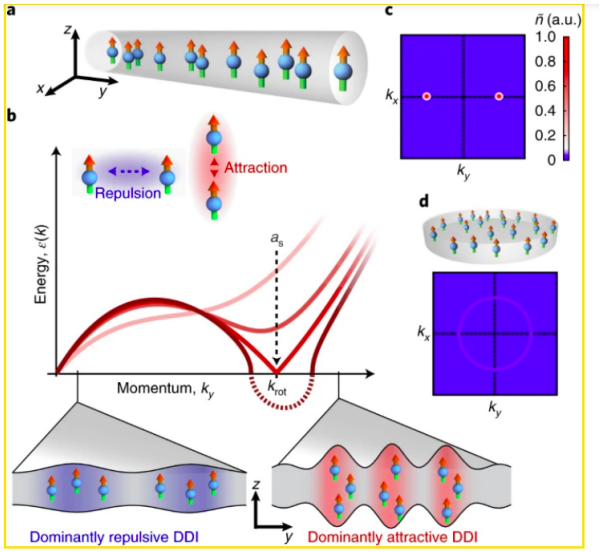

Figure 2.2: Figure (a) and (c) are for axial geometry while (d) is for a disc/pancake geometry. As one can see in (b), depending on the interaction strength of dipolar and contact interaction, dipoles can orient themselves on top of each other (dominantly attractive regime) and thus soften the excitation spectra, inducing a maxima (maxon) and a minima (roton). This roton gap can be tuned [4] to lower to down to zero and populate the roton modes. Its signatures is easily seen in (c) for axial geometry and (d) for pancake geometry.
Figure Courtesy: *Chomaz et. al. [4]*

discussed in 1.4.2 but with transverse width l_z also as a parameter, we get the following dispersion relation for all dipoles pointing out of the pancake

$$\epsilon(k)^{2D} = \sqrt{\frac{\hbar^2 k^2}{2m}\left(\frac{\hbar^2 k^2}{2m} + 2n_{2D}\left[g + \frac{8\pi g_d}{3} f\left(\frac{k l_z}{\sqrt{2}}\right)\right]\right)} \tag{2.5}$$

where, $f(x) = 1 - \frac{3\sqrt{\pi}}{2}|x| \exp[x^2] \operatorname{erfc}[x]$. Note that for appropriate values of g and g_d, we can get a minima in the dispersion relation at intermediate value of k. Futher, this can lead to imaginary value of excitation energy - *roton instability* (see figure).

2.3 Other Special Features in Dipolar BECs

There is no lack of odd structures in BECs with just isotropic contact interactions. We have quantized vortices and vortex arrays as excited states, predicted long back by Onsager (1949) and Feynman (1955) while trying to study superfluids. Scissor modes in atomic BEC [41, 42], creating an array of Josephson junctions [43] were all realised in atomic BECs with delta potential scatterings only. A dipolar BEC (DBEC) has even more of novel features, some particular examples of which will be listed below. Mostly, long-range character and anisotropy lead to some interesting correlations in the system [2, 3].

Magneto-restriction

In trapped condensates, consider a 3D Simple Harmonic potential for V_{ext} in equation 1.23, one finds that the condensate elongates along the direction of polarization [44–46]. It may seem counter-intuitive from inter-particle interaction perspective as the dipoles along the polarization direction, say z, tend to attract. However, looking the the energy landscape one finds that ground state corresponds to a condensate elongated along z.

Geometric stabilisation of trapped condensate

A BEC in harmonic trap can be stabilised even with effectively attractive interaction due to quantum pressure from zero point energy state of the trap. For a dilute gas with no dipolar interactions, the above is valid for the criteria

$$\frac{N|a|}{a_{\text{ho}}} \leqslant 0.58, \tag{2.6}$$

where $a_{\text{ho}} = \sqrt{\hbar/(m\omega)}$ of an isotropic trap with frequency ω. However, in a polarised dipolar condensate, one can make the confinement flat, like a pancake, and have the dipoles point

out of the pancake geometry as in figure below. This simply reduces the instances where dipoles are oriented top to bottom and thus, enhances stability.

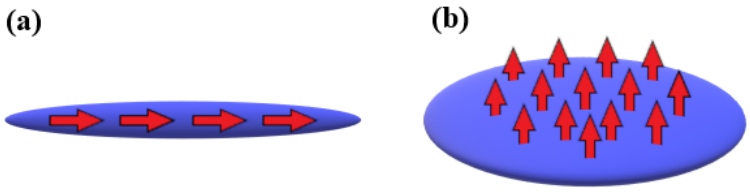

Figure 2.3: In (a) dipoles are mainly attracting each other, while in (b) they repel.

Vortex structures

In a rotating dipolar BEC one can study the properties of a single vortex, or of a vortex lattice. The angle between rotation axis and the polarization determines the vortex profile, whether crater-like - same direction, or elliptical - when orthogonal [47] and the lattice loses its hexagonal symmetry.

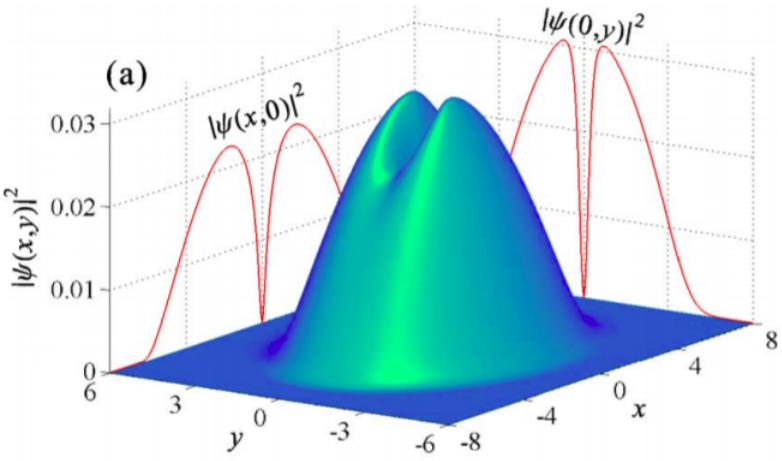

Figure 2.4: Here, the polarization is along x and roation is about the z axis. The eliptical shape of the vertex is evident.
Figure Courtesy: *Yi and Pu [47]*

Rosensweig Instability

A classical ferromagnetic fluid undergoes Rosensweig instability and creates self-organised structures. A DBEC is is a quantum ferromagnetic superfluid. We will present two instances of demonstration of Rosensweig instability.
One, induce a roton instability by tuning the effective interaction via Feshbach resonance. Now, one observes spontaneous patterns forming in the Dipolar BEC's ground state configuration [48] (see figure 1.5). If the superfluid flow is maintained, this would qualify as a ground state supersolid.
Two, one can find ferrofluidic behaviour on the interface of a 2-component dipolar BEC with one magnetised, and other not [49].

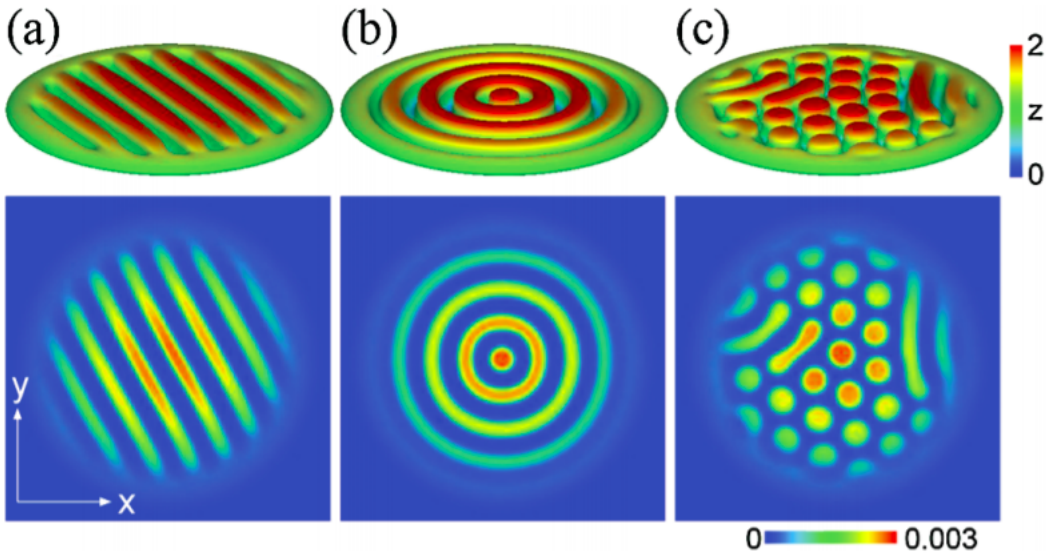

Figure 2.5: Simply by changing the initial seed in the imaginary time evolution, such density patterns were obtained in the the magnetic components surface.
Figure Courtesy: *Saito, Kawaguchi and Ueda [49]*

2.4 Interlayer effects in DBECs

Long-range nature of Dipolar interactions has opened a new avenue to study - interlayer Dipolar effects. Recent results point to obtaining various phases in Bose gases with just dipole-dipole interactions. Unless one uses inter-layer effects, such stabilisation of different

phases is not possible with just dipolar effects [50]. The interlayer configurations can form dipolar chains in a multi-stacked pancake system, just like classical magneto-fluids, and drastically change the condensation temperature [51]. The stability of an array of dipolar condensates in lattice has also been experimentally studied and phenomenon of dipolar stabilisation and destabilisation was studied [52]. In case of 2D solitons in parallel layers, one finds that long-ranged dipolar interaction induces an effective potential for the solitons to scatter. The results can be inelastic collisions or formation of soliton molecules [53]. Stability and formation of Q-1D soliton molecules, laid along each other has also been discussed [54]. Effective potential created by multi-stacked pancakes [55] and in-phase and out-of-phase oscillations in a lattice of pancakes places side by side have also been studied. Out-of-phase modes have been shown to be heavily dependent on dipolar potential [56]. Studies have also shown that interlayer effects can enhance roton instability regime [57, 58]. Effects of weak disorder potential in a 2D bilayer in parallel and anti parallel dipole orientation has also been studied.

Chapter 3

Results (I) - Interlayer induced confinement

In experiments concerning BEC, one typically forms a condensate inside an optical trap. Even the so-called 'uniform condensates' are actually made in very shallow traps. The light-matter interaction creates an effective potential for the atoms [59, 60]. To cool a cloud to micro or nano-Kelvin levels, one must restrict the momentum of cloud in all three directions. For that, at least six lasers are required, paired up against each other with polarisation orthogonal to each other.

Here, we propose a method to trap cigar shaped condensates, without using an external potential in the longitudinal direction from a laser cooling apparatus. That is, as discussed in 1.4.2 on prolate shaped condensates, there will be laser traps in the x and y directions, but the z direction will not require any laser to trap the condensate. We propose to achieve the entrapment using interlayer effects between Dipolar condensates. In later chapters we will see that the resultant condensate now has a very non-trivial matter wave profile which is a mimic of the sought-after supersolid state of matter. In this chapter, we discuss how inter-layer dipole-dipole interactions (DDIs) introduce entrapment in dipolar Bose-Einstein condensates. Our result demonstrates this in a bilayer system with three DBECs. In one layer, we have two trapped Q-1D condensates, where as in the second layer we have an untrapped one. With a proper choice of dipole orientations, the inter-layer DDIs effectively form a trapping potential for the condensate in the second layer with non-trivial patterns.

3.1 The System

In this section, we will introduce the system and its model. The general mean-field equations (GPE) will be given with the assumptions taken to justify their validity.

3.1.1 Model

To demonstrate the proposed entrapment, consider the following bilayer system as depicted in figure 3.1. The condensates have been labelled as ψ_1, ψ_2 and ψ_3. All three condensates are Quasi-1D, i.e. there is a cylindrically symmetric Harmonic potential $\frac{1}{2}m\omega_\perp^2 r^2$, in the axial direction $\hat{\mathbf{r}}$, which gives them the cigar shaped profile. In the upper layer, ψ_1 and ψ_2 are entrapped in shallow longitudinal lasers, represented by the green arrows in figure 3.1. The effective potential along the longitudinal, henceforth called z axis, is $\frac{1}{2}m\omega^2(z+\xi)^2$ for ψ_1 and $\frac{1}{2}m\omega^2(z-\xi)^2$ for ψ_2. ξ is the center of traps along the z axis and the condensates, ψ_1 and ψ_2 are expected to be centered around that position only. For, Q-1D regime, we would have $\frac{\omega_\perp^2}{\omega^2} >> 1$ and both layers are to be separated by a distance $y = \delta$ - large enough to rule out any overlap between all three condensates.

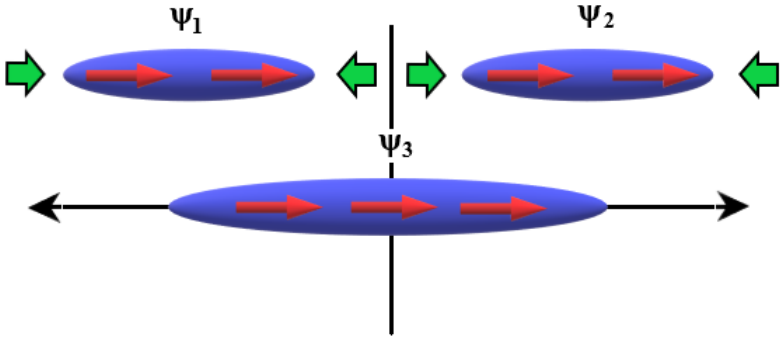

Figure 3.1: : This a schematic of the system. All three condensates are in a cylindrically symmetric trap of frequency $\omega_\perp$. This is supposed to provide a tight trap in the axial direction to each condensate and thus allow one to take a Q-1D approximation for the resultant prolate BECs. The dipoles are polarised with an external magnetic field such that all of them point in the $\hat{z}$ direction. ψ_1 and ψ_2 are held fixed along z axis by traps of frequency ω, shallower than axial direction. We claim to show that such configuration leads to induced entrapment of ψ_3 along the z axis.

Throughout the thesis, we would only deal with a fixed dipole polarisation along the $\hat{\mathbf{z}}$ direction. For the untrapped (longitudinally untrapped in Q-1D regime) condensate ψ_3, only the z degree of freedom is accessible. So, the expected ground state configuration would be for it to lay down in the center, as the repulsions between dipoles when being right below the upper layer condensates is unfavourable energy-wise and attractive forces act up when going too far away. Basically, one expects ψ_3 to settle down around $z = 0$.

We shall be working in the non-soliton, stable regime in what follows. Thus the entrapped condensate is stable against excitations, unlike the bright solitons seen previously. We shall soon quantify it using numerical and variational calculations. For now, let us have a look at the governing equations to our model.

3.1.2 The Governing Equations

We study the behaviour of this system in the mean-field limit using Gross-Pitaevskii Equations. To start off, we recall the 3D GPE:

$$i\hbar\partial_t\psi(\mathbf{x},t) = \left[-\frac{\hbar^2}{2m}\nabla^2 + V(\mathbf{x}) + g|\psi|^2 + \left(V_{\text{dd}} * |\psi|^2\right)\right]\psi(\mathbf{x},t), \qquad \mathbf{x}\in\mathbb{R}^3, t>0 \tag{3.1}$$

$V(\mathbf{x})$ is the external potential - a one-body operator. This is the effective resultant of the light-matter dipole coupling from lasers. $g = \frac{4\pi\hbar^2 a_s N}{m}$ is the contact interaction - a local, two body interaction which is elastic by definition and is proportional to s-wave scattering length a_s. N here is to be substituted with number of Bosons in the condensate. $V_{\text{dd}}(\mathbf{x}) = g_d\frac{1-3\cos^2(\theta)}{|\mathbf{x}|^3}$ is the classical expression for two magnetic (or electric) point dipoles separated by vector $\mathbf{x}$ and θ is the angle between $\mathbf{x}$ and the dipole moment. $g_d = \frac{\mu_0\mu_{\text{dip}}^2 N}{4\pi}$ where, μ_0 and μ_{dip} are vacuum magnetic permeability and permanent magnetic dipole moment respectively. To tackle such equations, one mostly resorts to numerical simulation. For that, we would start off with making the equation non-dimensional by scaling all relevant parameters in units suitable and sensible to the dynamics of the system at the energy scales involved. A detailed discussion is in references [12, 15], and a quick review in Appendix B.

First we re-write the equation in terms of the following parameters: $t_s = \frac{1}{\omega_\perp}$, $x_s = \sqrt{\frac{\hbar}{m\omega_\perp}} = l_\perp$ and $E_s = \hbar\omega_\perp$. Here, $\omega_\perp$ is radial trap frequency in 3.1. Scaling using this was

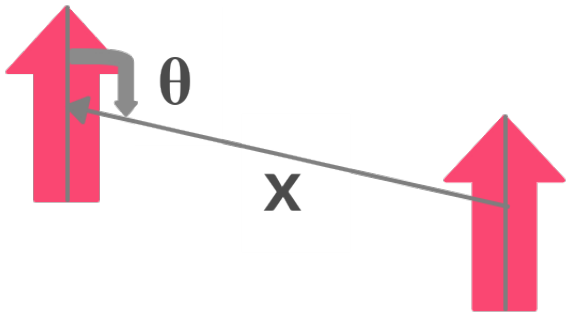

Figure 3.2: : The red arrows represent two point magnetic dipoles separated by $\mathbf{x}$ and θ is the angle between $\mathbf{x}$ and dipole axis as seen in the figure. The anisotropy is evident here. Even in the polarised dipoles scenario, different values of θ, change the nature of interaction from repulsive (e.g. $\theta = \pi/2$) to attractive (e.g. $\theta = \pi$).

found to be a convenient choice of units.

Then, assume that the three condensates we have, ψ_3 in lower layer and ψ_1, ψ_2 in upper layer are all 'well separated' and non-overlapping. This allows us to break the one dimensionless 3D GPE into three separate equations for each of the condensate. These three equations are coupled with the long range interaction term only. This is similar to multi-layer condensates mentioned in section 2.4. Now we have equations to simulate our system in full 3D, without making the Q-1D approximation 1.4.2. However, we shall justify in subsequent chapters that Quasi-1D is indeed a good approximation, by comparing numerical results. We get a set of three coupled equations which describe the condensate physics in 3D.

$$\begin{aligned} i\partial_t \psi_{1,2}(\mathbf{r},t) = &\left[-\frac{1}{2}\nabla^2 + V_{1,2}^{ext}(\mathbf{r}) + \tilde{g}\left|\psi_{1,2}(\mathbf{r},t)\right|^2 \right. \\ &\left. + \tilde{g_d} \int d^3\mathbf{r}' \left[\sum_{i=1}^{3} n_i(\mathbf{r}') \frac{1 - 3cos^2(\theta)}{(\mathbf{r}-\mathbf{r}')^3} \right] \right] \psi_{1,2}(\mathbf{r},t) \end{aligned} \tag{3.2}$$

and for ψ_3

$$\begin{aligned} i\partial_t \psi_3(\mathbf{r},t) = &\left[-\frac{1}{2}\nabla^2 + V_3^{ext}(\mathbf{r}) + \tilde{g}\left|\psi_3(\mathbf{r},t)\right|^2 \right. \\ &\left. + \tilde{g_d} \int d^3\mathbf{r}' \left[\sum_{i=1}^{3} n_i(\mathbf{r}') \frac{1 - 3cos^2(\theta)}{(\mathbf{r}-\mathbf{r}')^3} \right] \right] \psi_3(\mathbf{r},t) \end{aligned} \tag{3.3}$$

Things to take note of here are:

$$V_{1,2}^{ext}(\mathbf{r}) = 1/2\left[\omega_\perp^2 x^2 + \omega_\perp^2 (y-\delta)^2 + \omega^2 (z \pm \xi)^2\right]$$
$$V_3^{ext}(\mathbf{r}) = 1/2\left[\omega_\perp^2 x^2 + \omega_\perp^2 y^2\right].$$

Here, $\tilde{g} := \frac{g}{\hbar\omega_\perp l_\perp^3}$ and $\tilde{g_d} := \frac{g_d}{\hbar\omega_\perp l_\perp^3}$. The rest of the terms like $\mathbf{r}$,t are also scaled by $x_s = l_\perp$ and t_s, while the euation itself divided by E_s. These are the dimensionless equations to simulate the our system under the approximation that (i) GPE is valid as discussed in chapter 2, and (ii) the condensates are non-overlapping.

If one further approximates validity of Q-1D regime as discussed in 1.4.2, then each of the above three equation reduces to simply a differential equation in z and t. As a small recap to dimension reduction: We can reduce dimensions from 3D to 1D and obtain a Quasi 1D GPE. When anisotropy is high enough, i.e. $\gamma^2 = \frac{\omega_\perp^2}{\omega^2} >> 1$, we can reduce the 3D equation to a 1-D equation in the weak interaction regime as seen in 1.4.2. Therefore, we write, $\psi(\mathbf{r},t) \approx \psi(z,t)\, G_0(x,y), \quad \mathbf{r} \in \mathbb{R}$, where G_0 is the 2D Gaussian SHO ground state in x and y direction. Finally, we put this in 3-D GPE and then after some manipulation multiply the LHS and RHS with $G_0(x,y)$ and integrate over x and y to obtain the following three coupled Q-1D equations:

$$i\partial_t \psi_{1,2}(z,t) = \Bigg[-\frac{1}{2}\partial_{zz} + \frac{(z \pm \xi)^2}{2\gamma^2} + \tilde{g}^{1D}\left|\psi_{1,2}(\mathrm{z},t)\right|^2 + \sum_{(i,j)} \frac{\tilde{g}_d^{1D}}{3} \int dk_z e^{\iota k_z z} \hat{n}_i(k_z)\, F_j(k_z,\delta)\Bigg] \psi_{1,2}(\mathrm{z},t) \quad (3.4)$$

and for ψ_3, without any trap in Q-1D, we have

$$i\partial_t \psi_3(z,t) = \Bigg[-\frac{1}{2}\partial_{zz} + \tilde{g}^{1D}\left|\psi_3(\mathrm{z},t)\right|^2 + \sum_{(i,j)} \frac{\tilde{g}_d^{1D}}{3} \int dk_z e^{\iota k_z z} \hat{n}_i(k_z)\, F_j(k_z,\delta)\Bigg] \psi_3(\mathrm{z},t). \quad (3.5)$$

where,

$$F_j(k_x,\delta)=\int\frac{dk_ydk_z}{\pi}\left(\frac{3k_x^2}{k_x^2+k_y^2+k_z^2}-1\right)e^{-\frac{1}{2}\left(k_y^2+k_z^2\right)-\iota k_y j\delta} \tag{3.6}$$

The parameters in the system of equation are redefined in suitable dimensionless form: $\tilde{g}^{1D}=\tilde{g}/(2\pi)$ and $\tilde{g}_d^{1D}=\tilde{g}_d/(2\pi)$. In terms of physical quantities,

$$\gamma=\frac{\omega_\perp}{\omega},\quad \tilde{g}^{1D}=\frac{2a_sN}{x_s}\quad and\quad \tilde{g}_d^{1D}=\frac{m\mu_0\mu^2N}{8\pi^2\hbar^2x_s} \tag{3.7}$$

In the above equations, $\hat{n}_i\left(k_z\right)=\int dze^{-\iota k_z z}\left|\psi_i\right|^2$ and (i,j)th term represents the dipolar interaction with the i-th condensate. Value of j is either 0, 1 or -1 depending of the radial separation with i-th condensate. For 0 separation, e.g. ψ_1 with $i=1$ or 2 and $j=0$. Similarly, for 1δ (-1δ) separation between the layers, e.g. ψ_3 with $i=1$ or 2, and $j=1$ (-1 for reverse). In short, for condensates in same layer, j is 0 and for different, 1 (with -1 you get same answer).

Looking at equation 3.6, one can interpret that the $e^{-\iota k_y j\delta}$ term takes care of the displacement in y axis. Explicitly, such a term arises from the integral:

$$\int d\mathbf{r}'V_{dd}\left(\mathbf{r}-\mathbf{r}'\right)\left|\Psi\left(\mathbf{r}'\right)\right|^2=(2\pi)^3\int\hat{V}_{dd}(\mathbf{k})\hat{n}(\mathbf{k})e^{-\iota\mathbf{k}\cdot\mathbf{r}}d\mathbf{k}$$

This term gets multiplied by $\left|G_0(x,y)\right|^2$ when dimension reduction is being carried out and then integrated over y. $e^{-\iota k_y j\delta}$ arises since we are essentially Fourier Transforming a $shifted$ Gaussian.

3.2 Variational Analysis

A very efficient way to approximate the order parameter is to use variation principle on the expectation value of the Hamiltonian. One starts off with a trial wave-function, so called ansatz, and calculates the expectation value of the Hamiltonian. This trial wavefunction consists of some free parameters (e.g. variance and mean of a distribution). To calculate the approximate ground state, one can minimise the Energy expectation value taken with the ansatz, with respect to the free parameters. In case of solving for the order parameter, we

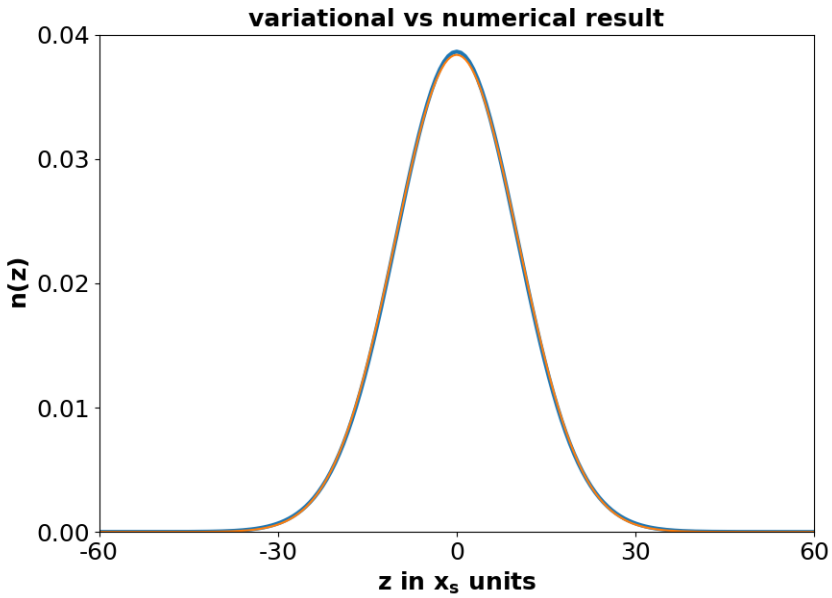

Figure 3.3: : 3D simulation of equation 4.2 with $\tilde{g} = 8.5$ and $\tilde{g}_d = 2.5$ in blue compared with a 3D Gaussian variation result in orange. Both results plotted after x and y variables were integrated out.

use the following energy expression.

$$E = \int \left[\frac{\hbar^2}{2m} |\nabla \Psi|^2 + V^{ext} |\Psi|^2 + \left(\frac{g}{2} |\Psi|^4 + \frac{g_d}{2} \int d^3\mathbf{r}' |\Psi(\mathbf{r}')|^2 \frac{1 - 3cos^2(\theta)}{(\mathbf{r} - \mathbf{r}')^3} |\Psi(\mathbf{r})|^2 \right) \right] \mathrm{d}^3\mathbf{r} \tag{3.8}$$

$$= E_{\text{kin}} + E_{\text{pot}} + E_{\text{int}} \tag{3.9}$$

In equation 3.8 we can use any guessed ansatz $\Psi(\{x_i\})$, where set of x_i can be any finite number of parameters. If the ansatz is a reasonable guess, and upon using suitable value of the parameters can indeed fit the ground state solution, we would have a very good analytical approximation of the ground state. This analytical nature of this variational approach is crucial to its usefulness. For BECs, a Gaussian ansatz or positive part of an inverted parabola (so-called Thomas-Fermi ansatz) are excellent approximations. In figure 3.3 one can see the excellent agreement between 3D numerical result and variational calculation done using a Gaussian with only variance as a variational parameter. Now, we shall apply the variational principle on equations 3.2 and 3.3. To do a variational calculation for a mean-field ground state. We start our analysis with a Gaussian ansatz, $\psi_i = A_i \mathbf{e}^{\sum_{\eta=\mathbf{x},\mathbf{y},\mathbf{z}} (\eta - \eta_\mathbf{i})^\mathbf{2} / (\mathbf{2L}^\mathbf{2}_{\mathbf{i},\eta})}$ to model

all the three condensates. A_i is just a constant satisfying $\int \psi_i^2 dx = 1$. Since, all we are interested is the ground state of the system of equations, we do it via minimisation of energy corresponding the given Hamiltonian in equations 3.2 and 3.3. That is,

$$\frac{E_{tot}}{\hbar\omega_\perp} = \sum_{i=1,2,3}\left[\sum_{\eta=x,y,z}\left[\frac{x_s^2}{4L_{i,\eta}^2} + \frac{L_{i,\eta}^2 + 2(\eta_i - \eta_i^{tr})^2}{4x_s^2\gamma_{i,\eta}^2}\right] + \frac{g x_s^{3/2}}{\hbar\omega_\perp 4\sqrt{2}\pi^{\frac{3}{2}} L_{i,x}L_{i,y}L_{i,z}} + \frac{f_i}{\hbar\omega_\perp}\right] + \sum_{i<j}\frac{h_{i,j}}{\hbar\omega_\perp} \tag{3.10}$$

where, $f_i = 1/(2(2\pi)^3)\int \hat{n}_i(\mathbf{k})V_{dd}(\mathbf{k})\hat{n}_i(-\mathbf{k})d^3k$, $h_{i,j} = 1/((2\pi)^3)\int \hat{n}_i(\mathbf{k})V_{dd}(\mathbf{k})\ \hat{n}_j(-\mathbf{k})d^3k$ and $\gamma_{i,\eta} := \omega_\perp/\omega_{i,\eta}$. Here, we have explicitly written down all the constants to be used for scaling for the convenience of the reader.

3.3 Soliton regime

Before we proceed to the analysis, we would like to conform the soliton regime. Our claim at the beginning of this chapter was to have an inter-layer dipolar interaction induce entrapment in a stable condensate. Being in the bright soliton regime would make the exercise not relevant anymore as we would anyway get self-entrapment, but with soliton instability (2.4). So, we must be careful and stay in non-soliton regime throughout our analysis.

Soliton regime using 3D variational calculation

As we have demonstrated in figure 3.3, solitons are excellently modelled via a Gaussian ansatz. To proceed we use equation 3.3 to model the condensate. This will be done using a 3D Gaussian ansatz with widths as variational parameters. The term to be minimised is thus

$$E_{sol} = \sum_{\eta=x,y,z}\frac{1}{4L_\eta^2} + \frac{L_x^2}{4} + \frac{L_y^2}{4} + \frac{\tilde{g}}{4\sqrt{2}\pi^{\frac{3}{2}}L_xL_yL_z} + \frac{1}{2(2\pi)^3}\int \hat{n}(\mathbf{k})\hat{V}_{dd}(\mathbf{k})\hat{n}(-\mathbf{k})d^3k \tag{3.11}$$

where $\hat{V}_{dd}(\mathbf{k}) = 4\pi\tilde{g}_d\left(k_z^2/||k||^2 - 1/3\right)$ and $\hat{n}(\mathbf{k})$ are Forward Fourier Transforms of $V_{dd}(\mathbf{r})$ and $n(\mathbf{r}) = |\psi(\mathbf{r})|^2$ in dimensionless units.

Next, we minimise equation 3.11 with respect to L_x, L_y and L_z. Signature of soliton is:

- a negative chemical potential given by $\mu = E_{kin} + 2E_{contact} + 2E_{dipolar}$. This criteria is easily deduced from time the independent GPE by taking inner product of both sides of GPE with ψ, the stationary state.
- finite value of width L_z. Practically, we can consider $L_z \leq O(10^3)$ as finite.

From the variational calculation we see clear indication of a phase transition. In figure 3.4, we have $\tilde{g} = 10.0$ fixed and we vary the value of $\tilde{g}_d$ each time and obtain the points. Soliton formation in DBEC is indeed a clear case of phase transition.

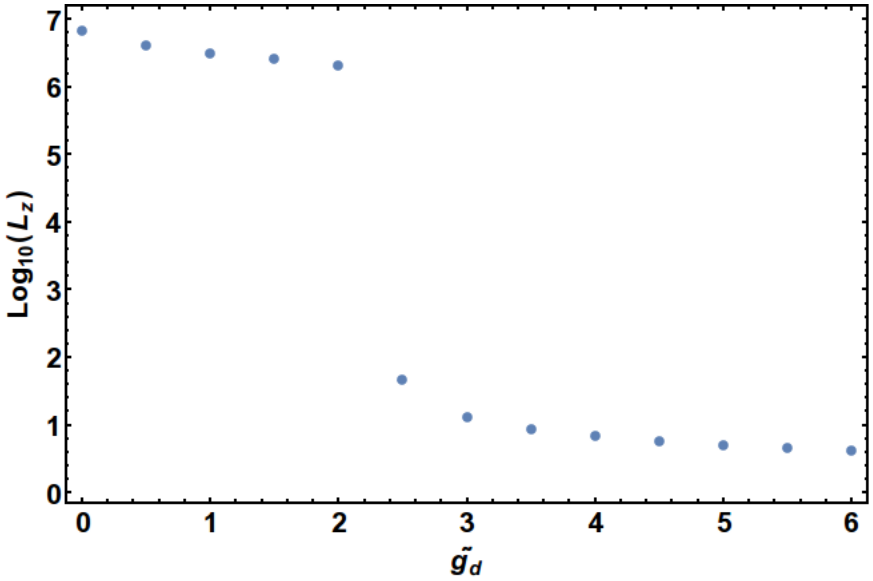

Figure 3.4: : In the obtained variational result, we have $\text{Log}_{10}L_z$ on y axis and $\tilde{g}_d$ on x axis. $\tilde{g} = 10$ is held fixed. The abrupt change indicates soliton formation between $\tilde{g}_d$ between 2 to 2.5 and thereafter.

Now we do the same we did for figure 3.4, but now with varying $\tilde{g}$ too. The results are shown in the following contour plot 3.5. In this plot, we have a contour for $L_z = O(10^6)$ at the boundary of green and blue region. Clearly, the blue region is a stable non-soliton regime. Even though this is not the best way to precisely pinpoint the soliton regime, we still are sure that at-least the blue region is stable. The phase boundary appears jagged however. This is actually not an accurate depiction as when checked minutely on case by case basis, the phase transition boundary between soliton and non-soliton regime is a straight line which

follows the Quasi-1D criteria with a uniform condensate approximation in equation 3.13 so well that we can consider them to give exact same results as far as our results and analysis are concerned.

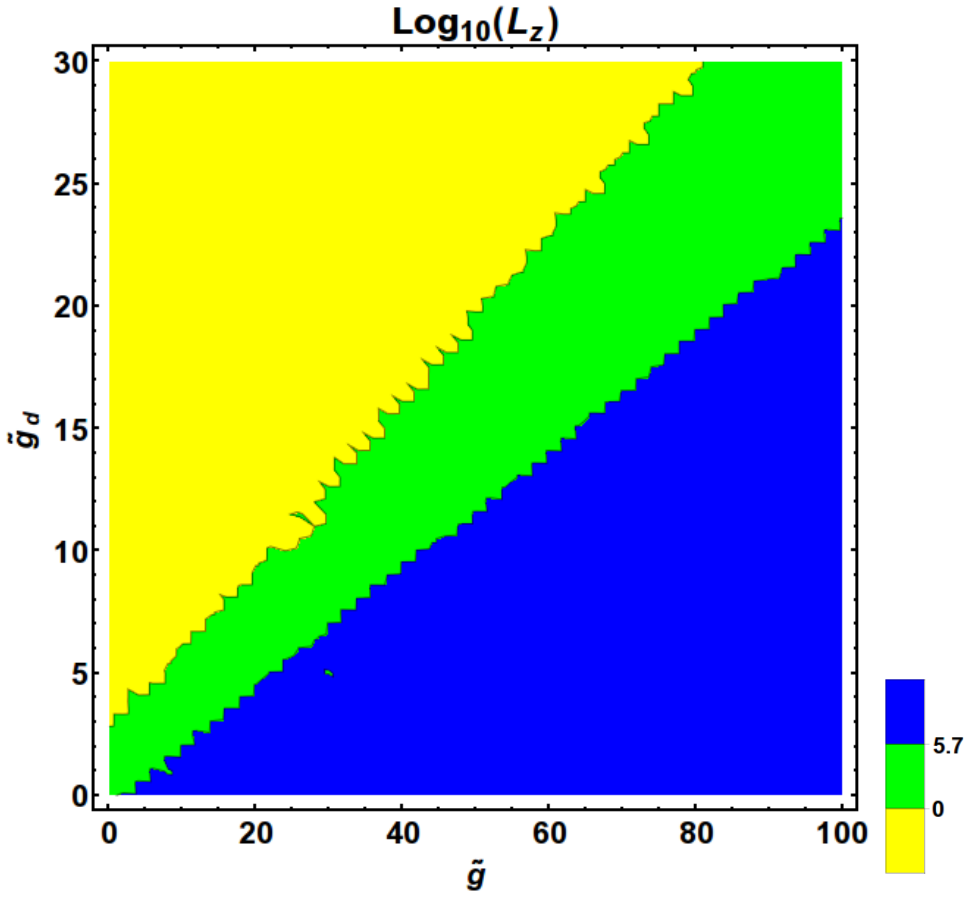

Figure 3.5: : This is a contour plot of $log_{10}L_z$ value of the variational ground state. The axes are the values of $\tilde{g}$ and $\tilde{g}_d$ for different scenarios. One can see that the blue region has $L_z \gtrapprox O(10^6)$, for green its mostly of $O(10^1)$ or $O(10^2)$. Yellow region is where condensate collapses i.e. even stabilty induced by geometric confinement is not enough to stabilise the condensate.

For the Q-1D estimate of soliton regime we start by assuming uniform density of the ground state solution:

$$\tilde{g}^{1D} n_0 + \frac{\tilde{g}_d^{1D}}{3} \int dk_z e^{\iota k_z z} \left(n_0 \delta(k_z) 2\pi\right) F_0\left(k_z\right) < 0 \tag{3.12}$$

$$\implies \tilde{g}^{1D} - \frac{\tilde{g}_d^{1D}}{3}(4\pi) < 0 \tag{3.13}$$

we find that the chemical potential $\mu^{1D} < 0$ for $\tilde{g}^{1D} < \tilde{g}_d^{1D} 4\pi/3$. This inequality has been verified to work as a very good estimate via numerical simulation as well as variational calculation of the energy landscape.

3.4 Variational Ground State estimates

We apply variational analysis on the Q-1D Hamiltonian of the system from the coupled equations 3.4 and 3.5. This gives us the following expression for energy of the system:

$$E_{1,2}^{1D} = \int \left[-\frac{1}{2} \left|\partial_x \psi_{1,2}\right|^2 + \frac{(x \pm \xi)^2}{2\gamma^2} \psi_{1,2}^2 + \frac{\tilde{g}^{1D}}{2} \left|\psi_{1,2}\right|^4 \right] dx + \sum_{(i,j)} \frac{\tilde{g}_d^{1D}}{3} \int dk_x \hat{n}_i \left(k_x\right) F_j \left(k_x, \delta\right) \hat{n}_{1,2} \left(-k_x\right) \quad (3.14)$$

and

$$E_3^{1D} = \int \left[-\frac{1}{2} \left|\partial_x \psi_3\right|^2 + \frac{\tilde{g}^{1D}}{2} \left|\psi_3\right|^4 \right] dx + \sum_{(i,j)} \frac{\tilde{g}_d^{1D}}{3} \int dk_x \hat{n}_i \left(k_x\right) F_j \left(k_x, \delta\right) \hat{n}_3 \left(-k_x\right) \quad (3.15)$$

Clearly, Total Energy is, $E_{tot}^{1D} = E_1^{1D} + E_2^{1D} + E_3^{1D}$ and of course, E_i^{1D} doesn't mean much except for notational convenience. We shall put in our Gaussian ansatz $\psi_i = A_i \mathbf{e}^{\frac{(\mathbf{x}-\mathbf{x_i})^2}{\mathbf{2L_i^2}}}$ in E_{tot}, and get an expression for it in terms of width and centers of the three distinct Gaussians. Basically, we put $L_x = L_y = x_s$ in equation 3.10 and do the minimisation. All total we have six independent parameters to work with. Given the symmetry of the system, we do expect $x_3 = 0$, $x_2 = -x_1$, and $L_1 = L_2$. It is important to emphasize again that we will not be working in the soliton regime. So, if the upper pipe is taken out of the equation, we don't expect any confinement in the lower pipe. To get a condensate, one has to put laser traps along z directions too. Otherwise, the condensate will just disperse to give a uniform condensate in an $infinite$ box.

Upon Global Minimisation, if all values are finite with respect to the system size (particularly $0 < L_3 < \infty$), we do have a stable ground state with an inter-layer induced confinement in ψ_3. We ensure that by making $\tilde{g}^{1D} > \tilde{g}_d^{1D} 4\pi/3$ and also using calculations as in figure 3.5.

We shall fix a value of g_d and check for various parameter ranges of g_c to get a confined state. We always fix the separation between layers $\delta = 6$ to avoid any overlap between the two layers of condensate. We started off with $\gamma = 10$ and observed that for $\tilde{g}_d^{1D} \leq O(1)$ or lesser, the minimisation scheme becomes unreliable and we can't say for sure if we do have a global minima as we had expected previously. However, for $\tilde{g}_d^{1D} = O(10)$ we did confidently find a global minima for various values and configurations that will be explored in the next chapter.

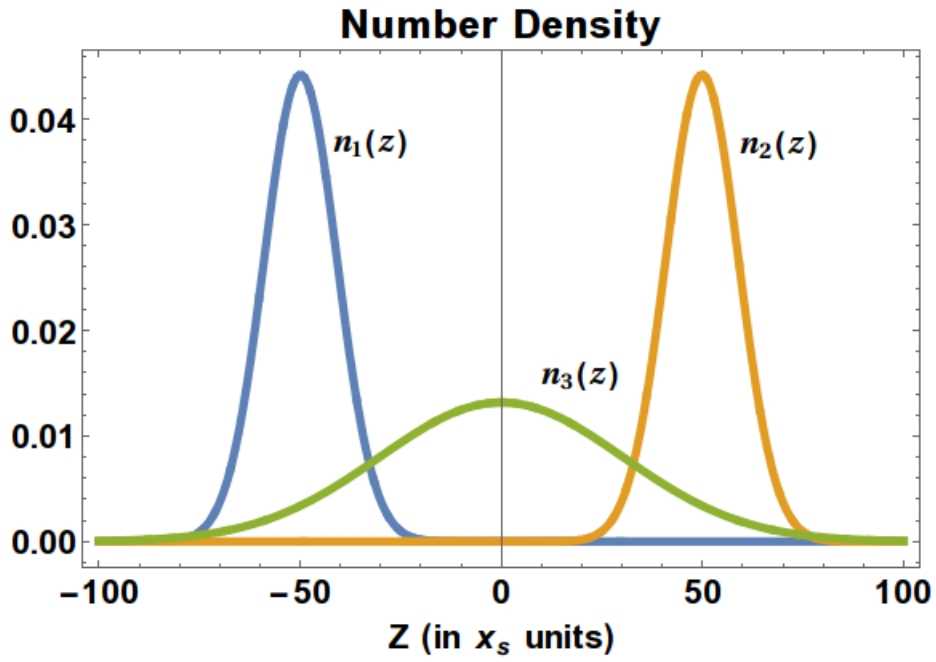

Figure 3.6: : Blue and Yellow curves represent $|\psi_1|^2$ and $|\psi_2|^2$ in the **upper** layer. The green curve is $|\psi_3|^2$ present in the **lower** layer. There is no overlap whatsoever, all three condensates are depicted together just for convenience of plotting them on the same z-axis, which is scaled in units of x_s, and nothing more. We have $\delta = 6x_s$, $\gamma = 10$, $\xi = 50.00x_s$, $\tilde{g}^{1D} = 100$ and $\tilde{g}_d^{1D} = 23$ and this the Global Minima for Total Energy Functional and hence, the "ground state" for Gaussian Variational Calculation using GPE.

For now we pick out one configuration as a proof of concept $\tilde{g}_d^{1D} = 23$ and $\tilde{g}^{1D} = 100$ we get inter-layer induced trapping in ψ_3 (see figure 3.6). We are way out of soliton regime by any estimates. According to figure 3.5 and equation 3.13 for Q-1D calculations we are totally in stable configuration and the finite width of the $n_3(z)$ is only due to the dipole

interactions with the upper layer. We find that we can get desired confined solutions in a big range of values for $\tilde{g}_d^{1D}$ and $\tilde{g}^{1D}$. This will be explored in later chapters. As a note, it is very difficult to conclude to very small interaction parameters as the energy scale of interaction is very low. The interaction energy term responsible for self-confinement goes as $e^{-\delta^2}$ and that is already quite small compared to intra-dipolar energy with no such relative suppression.

Finally, we present the detailed results. The configuration is $\delta = 6$, $\gamma = 10$, $\xi = 50.00$, $\tilde{g}_c^{1D} = 100$ and $\tilde{g}_d^{1D} = 23$. The global minima is given by $L_1 = L_2 = 9.03x_s$, $L_3 = 30.28x_s$, $x_2 = -x_1 = 49.98x_s$ and $x_3 = 0.00$. Everything has been just as expected, with only a word of caution to not keep ξ too small, as, the attraction between ψ_1 and ψ_2 can be enough to overcome the two Gaussian wells in the upper pipe and thus, *may* take away the global minimum. The uncertainty in previous statement is for the fact that our equations can only handle the non-overlapping regime. They simply breakdown for the scenario above and any values calculated by them could just be rubbish.

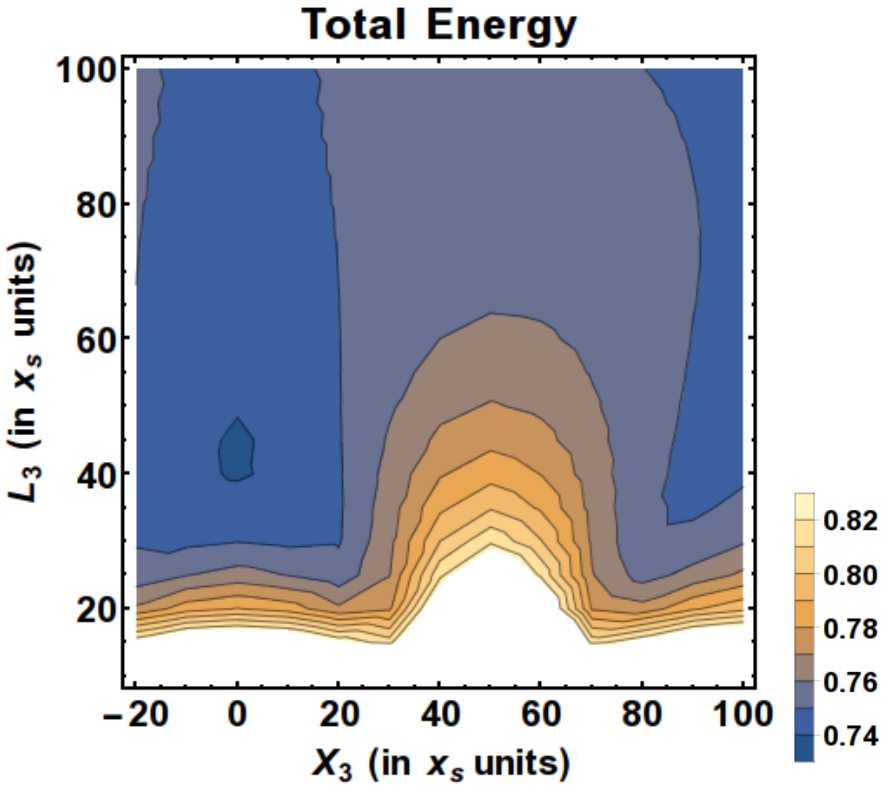

Figure 3.7: :Contour Plot for Total Energy of the system with $L_1 = L_2 = 9.03x_s$, and $x_2 = -x_1 = 49.98x_s$ fixed and the only variables being (L_3, x_3).

To establish the global minima, we varied all present 6 parameters and verified the

calculated value of total energy E_{tot}^{1D}. Here, we also present contour plot of Energy with $L_1 = L_2 = 9.03x_s$, and $x_2 = -x_1 = 49.98x_s$ fixed. The two variables are thus the width of the third condensate and its position on the z-axis, i.e. E_{tot}^{1D} vs (L_3, x_3).

In this configuration, $E_1^{1D} = E_2^{1D} = 0.36$, $E_3^{1D} = -0.0077$, $\mu_1^{1D} = \mu_2^{1D} = 0.52$ and $\mu_3^{1D} = -0.0158$. It doesn't seem to strictly follow the the criteria we set for applicability of dimension reduction, i.e. $\mu^{1D} << 1$. But, for ψ_3 it sure does. Also, even with 3D variational calculations, we got the same result. Since, ψ_1 and ψ_2 are confined in Harmonic traps, we don't expect their profiles to vary much from Gaussian Ansatz calculation anyway. Surprisingly, the Gaussian Ansatz is not the most excellent choice for ψ_3. Numerical analysis will reveal that in the next chapter.

3.5 Summary

So, we seem to have achieved inter-layer induced confinement in a stable condensate from the variational calculation. We emphasize that this is a form of indirect control over an otherwise unconfined condensate via interlayer dipolar interactions. This allows the study and formation of a cigar-shaped condensate in a non-soliton regime without any optical traps in the longitudinal direction. One has control over the width of ψ_3 just by manipulating parameters in the upper layer's condensates, e.g., through ξ, changing numbers of bosons in the upper layer's condensate and what not! The next step is to simulate the GPE numerically, and the results are non-trivial and novel.

Chapter 4

Results (II) - Interlayer induced density modulations

As demonstrated in the previous chapter, we can achieve inter-layer induced confinement due to dipole-dipole interaction's long-range and anisotropic nature. But, just as we hinted at earlier, the ground state on the condensate, which is made confined, is non-trivial. Condensate ψ_3 in the lower layer of figure 3.1 has got its density profile modulated due to the anisotropic inter-layer dipolar interaction. In typical BEC experiments, one can get density modulated BEC in the following ways: (i) Tuning the interference of counter-propagating laser with control over the populations of the bosons in the coupled states. Manipulating interference and polarisation of lasers can carve out a potential landscape. (ii) One can populate the roton mode [4]. This leads to periodic modulations in density corresponding to the frequency of the roton mode. Mean-field theory predicts roton-maxon instability, but beyond *mean field theory*, shows formation of droplets and a superfluid background.

It is important to recall that the stability of BECs, dipolar or otherwise, strongly depends on the configuration of the laser trap. It is no longer a simple matter-wave in free space. Also, as we saw in equation 2.5 for Q-2D condensate and section 2.2.2, roton mode leads to roton-maxon instability. And to invoke beyond mean-field effects, a precise balance between the parameters and ramping them high enough to make Quantum Fluctuations take over. is required.

We propose in this chapter to achieve density modulated structures with the help of

dipole-induced interactions from the upper layer to the lower layer as in figure 3.1. This induced inter-layer confinement and density modulation are in a stable BEC without any optical trap along the length of the layers. Further, as we will show soon, this scheme of inducing density modulations opens up new non-trivial structures in a matter-wave in free space. These structures are easily manipulated and tuned by changing the configuration in the upper layer. The coherence between the density peaks can also be controlled.

4.1 A Brief Overview

Let us take a quick recap of the system. In the following schematic 4.1, we have a bi-layer system with orientation of dipoles as in the figure. All condensates are in cylindrical traps to create prolate geometry.

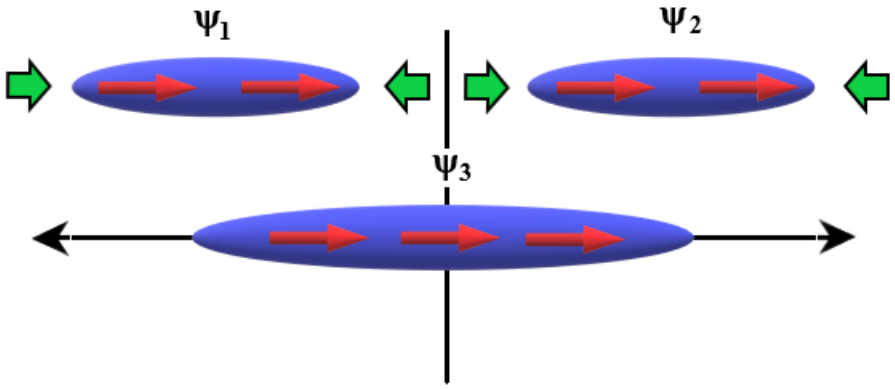

Figure 4.1: : This a schematic of the system. All three condensates are in a cylindrically symmetric trap of frequency $\omega_\perp$. This is supposed to provide a tight trap in the axial direction to each condensate and thus allow one to take a Q-1D approximation for the resultant prolate BECs. The dipoles are polarised with an external magnetic field such that all of them point in the $\hat{z}$ direction. ψ_1 and ψ_2 are held fixed along z axis by traps of frequency ω, shallower than axial direction. Such configuration can lead to induced entrapment of ψ_3 along the z axis.

We shall be working in the non-soliton, stable regime in what follows. One expects ψ_3 to settle down around $z = 0$. We have already seen how we can achieve inter-layer induced

entrapment. Now, we will employ numerical simulation of GPE to get the ground state. The equation to follow are the same 3.2 - 3.3.

$$i\partial_t\psi_{1,2}(\mathbf{r},t) = \left[-\frac{1}{2}\nabla^2 + V_{1,2}^{ext}(\mathbf{r}) + \tilde{g}\left|\psi_{1,2}(\mathbf{r},t)\right|^2 + \tilde{g_d}\int d^3\mathbf{r}'\left[\sum_{i=1}^{3} n_i(\mathbf{r}')\frac{1-3cos^2(\theta)}{\left(\mathbf{r}-\mathbf{r}'\right)^3}\right]\right]\psi_{1,2}(\mathbf{r},t) \tag{4.1}$$

and for ψ_3

$$i\partial_t\psi_3(\mathbf{r},t) = \left[-\frac{1}{2}\nabla^2 + V_3^{ext}(\mathbf{r}) + \tilde{g}\left|\psi_3(\mathbf{r},t)\right|^2 + \tilde{g_d}\int d^3\mathbf{r}'\left[\sum_{i=1}^{3} n_i(\mathbf{r}')\frac{1-3cos^2(\theta)}{\left(\mathbf{r}-\mathbf{r}'\right)^3}\right]\right]\psi_3(\mathbf{r},t) \tag{4.2}$$

where the traps are as follows

$$V_{1,2}^{ext}(\mathbf{r}) = 1/2\left[\omega_\perp^2 x^2 + \omega_\perp^2(y-\delta)^2 + \omega^2(z\pm\xi)^2\right]$$
$$V_3^{ext}(\mathbf{r}) = 1/2\left[\omega_\perp^2 x^2 + \omega_\perp^2 y^2\right].$$

We have parameters such that Q-1D approximation should work (see section 1.4.2 for more on Q-1D). We will also verify that by directly comparing both simulations and present the results. For Q-1D, the equations are the same 3.4 - 3.5

$$i\partial_t\psi_{1,2}(z,t) = \left[-\frac{1}{2}\partial_{zz} + \frac{(z\pm\xi)^2}{2\gamma^2} + \tilde{g}^{1D}\left|\psi_{1,2}(\mathrm{z},t)\right|^2 + \sum_{(i,j)}\frac{\tilde{g}_d^{1D}}{3}\int dk_z e^{\iota k_z z}\hat{n}_i\left(k_z\right)F_j\left(k_z,\delta\right)\right]\psi_{1,2}(\mathrm{z},t) \tag{4.3}$$

for ψ_3, without any trap in Q-1D, we have

$$i\partial_t\psi_3(z,t) = \left[-\frac{1}{2}\partial_{zz} + \tilde{g}^{1D}\left|\psi_3(\mathrm{z},t)\right|^2 + \sum_{(i,j)}\frac{\tilde{g}_d^{1D}}{3}\int dk_z e^{\iota k_z z}\hat{n}_i\left(k_z\right)F_j\left(k_z,\delta\right)\right]\psi_3(\mathrm{z},t). \tag{4.4}$$

That is all we need to proceed.

4.2 Calculating Ground State of GPE

To calculate the Ground State of a GPE, we present the numerical scheme in Appendix A (A). An extra step we take to get the ground state is to iterate A.5 with imaginary time i.e. $it \to t$ in the expressions for time evolution operators $\hat{U}_r$ and $\hat{U}_k$. Further, in 3D GPE, the dipole term is implemented as

$$\tilde{g}_d \int d^3\mathbf{r}' \left[n(\mathbf{r}') \frac{1 - 3cos^2(\theta)}{(\mathbf{r} - \mathbf{r}')^3} \right] = \frac{4\pi}{3} \tilde{g}_d F T_{3D}^{-1} \left[\hat{n}_j(\mathbf{k}) \left(\frac{3k_z^2}{\mathbf{k}^2} - 1 \right) \right] \tag{4.5}$$

. For Q-1D equation 4.3 - 4.4 the integral in dipolar term is clearly implementable by an Inverse Fourier Transform. To do the Fourier Transforms, we used FFTW package for C[1].

4.3 The modulated Ground State

Here we present the result out of simulating the 3D mean-field GPE for our system. In figure 4.2 and figure 4.3, we have plotted the iso-density contour of $n_3(\mathbf{r}) = |\psi_3(\mathbf{r})|^2$. The values of density is given in the color legends. The radial symmetry in $x - y$ and the longitudinal modulations in z is evident. As we mentioned in chapter 3, these numerical results also confirm the inter-layer induced confinement in stable, non-soliton regime. The condensates in upper layer ψ_1 and ψ_2 are nothing unexpected and follow the trap geometry with a density profile close to a Gaussian with widths corresponding to the traps.

The short description of parameters is:

1. for figure 4.2, $\delta = 6x_s$, $\gamma = 3$, $\xi = 40x_s$, $\tilde{g} = 42$ and $\tilde{g}_d = 10$. We are not in soliton regime. Increasing $\tilde{g}$ further till $\tilde{g} = 43$, thus going even further from soliton regime while increasing intra-layer repulsion between bosons, we confirmed that we get a solution of similar nature. Going further, the condensate's size starts increasing and

[1] http://www.fftw.org/

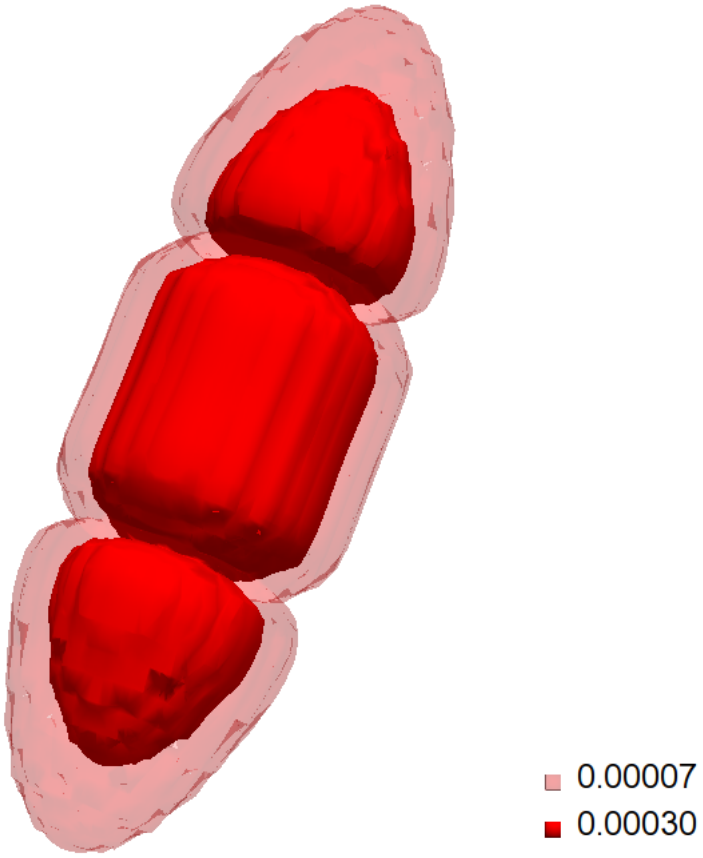

Figure 4.2: Contour Plot for number density of ψ_3 with system paramters $\delta = 6x_s$, $\gamma = 3$, $\xi = 40x_s$, $\tilde{g} = 42$ and $\tilde{g}_d = 10$. We are not in soliton regime. The condensate has depression in density close to $z = \pm\xi$ due to repulsion from upper layer dipoles. In center and to the sides, there is a bulge as the interlayer dipole interactions pushes the bosons in ψ_3 towards the equilibrium position. The value of $\mu = 0.999561$.

confinement is slowly lifted. Value of chemical potential $\mu = 0.999561$ and $1 - \mu = O(10^{-4})$.

2. for figure 4.3, $\delta = 6x_s$, $\gamma = 3$, $\xi = 40x_s$, $\tilde{g} = 420$ and $\tilde{g}_d = 100$. We are again, far from soliton regime. Just like before, increasing $\tilde{g}$ further away, the condensate's size starts increasing and confinement is slowly lifted. The value of $\mu = 0.994118$. Even with $\tilde{g}_d = 100$, we seem to satisfy Q-1D criteria.

The inter-layer dipole potential due to each condensate has two equilibrium positions around it for a point test dipole in lower layer. This roughly explains presence of slight dip

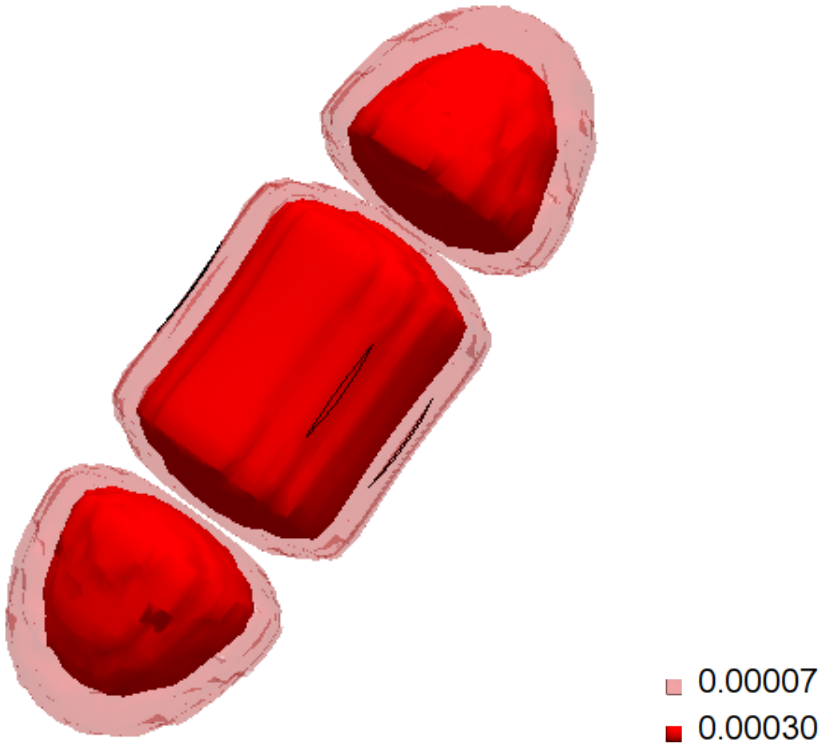

Figure 4.3: Contour Plot for number density of ψ_3 with system paramters $\delta = 6x_s$, $\gamma = 3$, $\xi = 40x_s$, $\tilde{g} = 420$ and $\tilde{g}_d = 100$. We are not in soliton regime. The condensate's depression in density at $z = \pm\xi$ is significantly more than in figure 4.3. This was expected as $\tilde{g}_d$ is significantly larger. In center and to the sides, there is a bulge again. But the situation is different too, in the sense that the peaks are less connected.

in the central bulge in figure 4.3. $\delta = 6x_s$ is fixed in both. The condensates have maintained their cylindrical symmetry in confirmation that we can make a Q-1D approximation. We will soon make direct comparisons.

4.3.1 A closer look at the structures

In this sub-section, we will plot column and disc integrated number densities of the condensates. We will also compare 3D GPE and Q-1D GPE results. The column densities are defined as $n_{CI}(y,z) = \int n(x,y,z)dx$ i.e. a marginalised probability distribution function (pdf) of number density. Similarly we have $n_{disc}(z) = \int\int n(x,y,z)dxdy$. We can directly

compare n_{disc} with Q-1D solution. Some plots of $n_{CI}(y,z)$ are discussed below:

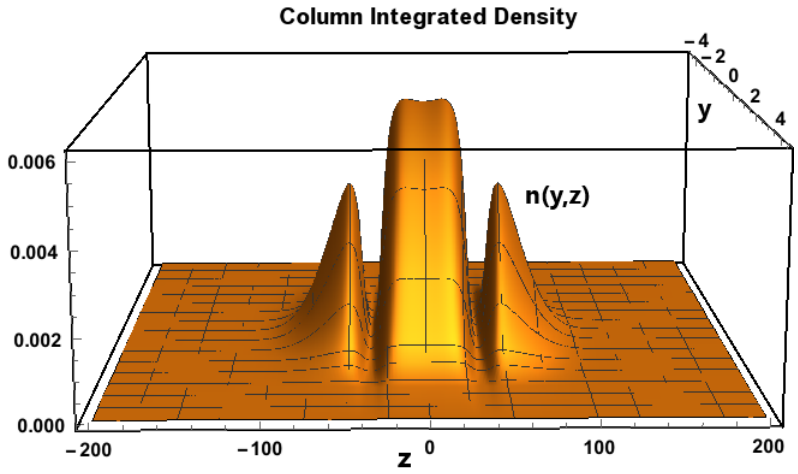

Figure 4.4: Plot for Column Integrated number density of $n_3^{CI}(y,z)$ with system paramters $\delta = 6x_s$, $\gamma = 3$, $\xi = 35x_s$, $\tilde{g} = 215$ and $\tilde{g}_d = 51$. We are not in soliton regime.

1. Figure 4.4: The slight dip in density at the condensate's center is prominently displayed here. Due to repulsion from ψ_1 and ψ_2 we see that the dip at $z = \pm\xi$ has very small density. We will see soon that as we increase the magnitude of dipolar interactions (by changing number of bosons, N) the density at dips keeps on vanishing.

2. Figure 4.5: Two prominent changes from (1). The slight dip in density at the condensate's center is replaced by a sharp peak as ξ is reduced to $25x_s$, and the dip at $z = \pm\xi$ is much shallower. $\tilde{g}_d = 5$ is ten times smaller than in case (1).

3. Figure 4.6: Only one parameter changed from (1). That is the value of ξ from $35x_s$ to $10x_s$. The effect however has pushed out most condensates towards the sides, out of the central lobe. Bringing ψ_1 and ψ_2 very close makes the position $z = 0$ at higher potential energy - in the sense of a test dipole description.

4. Figure 4.7: Only one parameter changed from (1) and (3). That is again, the value of ξ from $35x_s$ or $10x_s$ to $17x_s$ - in middle. As our analogy with point test dipole expects, here we see that the central is most prominent. The overall tendency is for dipoles to collect at center and not in the side lobes (as in 4.7), or just beside the center (as in 4.4) creating a dip in middle.

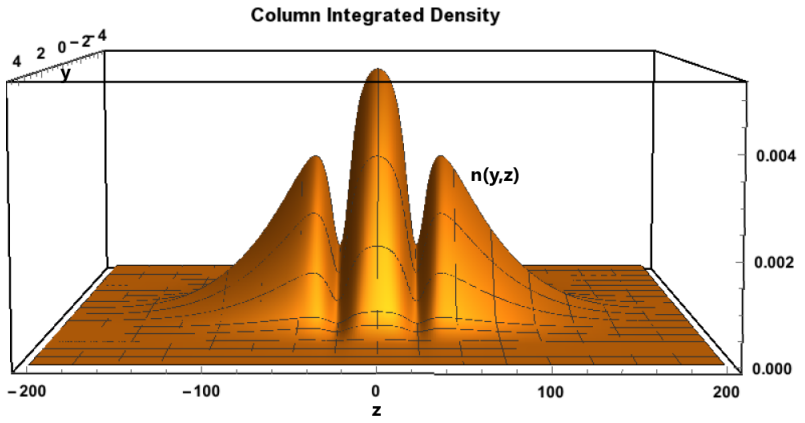

Figure 4.5: Plot for Column Integrated number density of $n_3^{CI}(y,z)$ with system paramters $\delta = 6x_s$, $\gamma = 3$, $\xi = 25x_s$, $\tilde{g} = 21$ and $\tilde{g}_d = 5$.

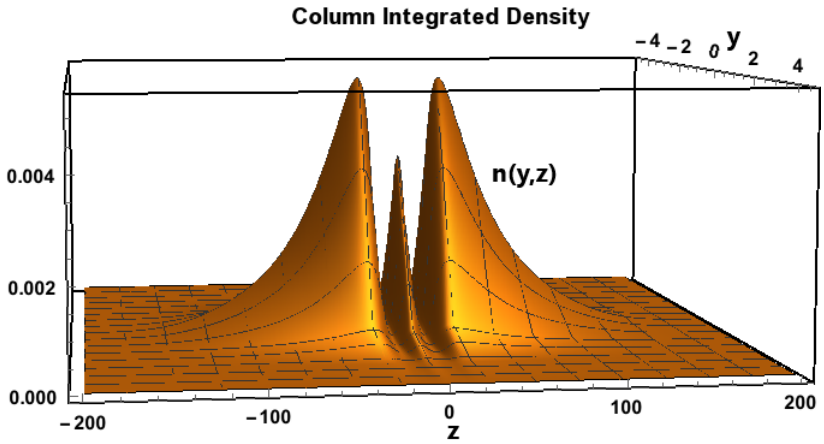

Figure 4.6: Plot for Column Integrated number density of $n_3^{CI}(y,z)$ with system parameters $\delta = 6x_s$, $\gamma = 3$, $\xi = 10x_s$, $\tilde{g} = 215$ and $\tilde{g}_d = 51$.

4.3.2 3D vs Quasi 1D solution

We saw in previous sub-section that value of $\mu/\hbar\omega_\perp \gtrapprox 0.99$. Since this is close to 1 as demanded in discussion on Q-1D regime - 1.4.2 (see also [15]), we do get another incentive to make the Q-1D approximation. First being the highly prolate geometry and cylindrical symmetry of the 3D ground state condensates.

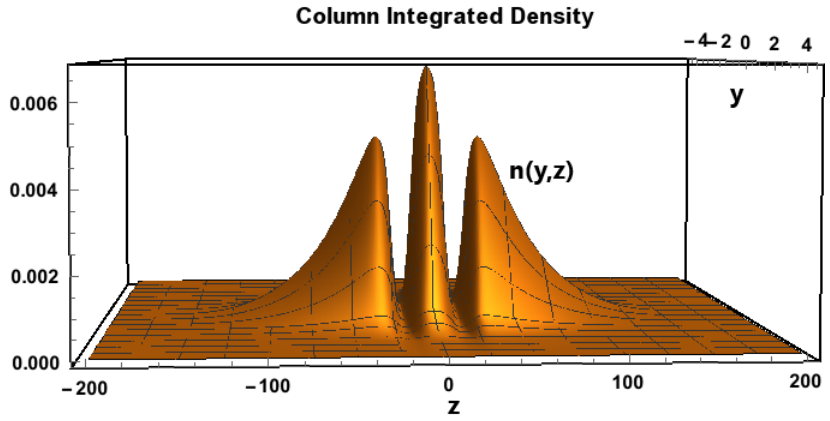

Figure 4.7: Plot for Column Integrated number density of $n_3^{CI}(y,z)$ with system parameters $\delta = 6x_s$, $\gamma = 3$, $\xi = 17x_s$, $\tilde{g} = 215$ and $\tilde{g}_d = 51$.

Some comparisons of the 3D and Quasi-1D solution are given below:

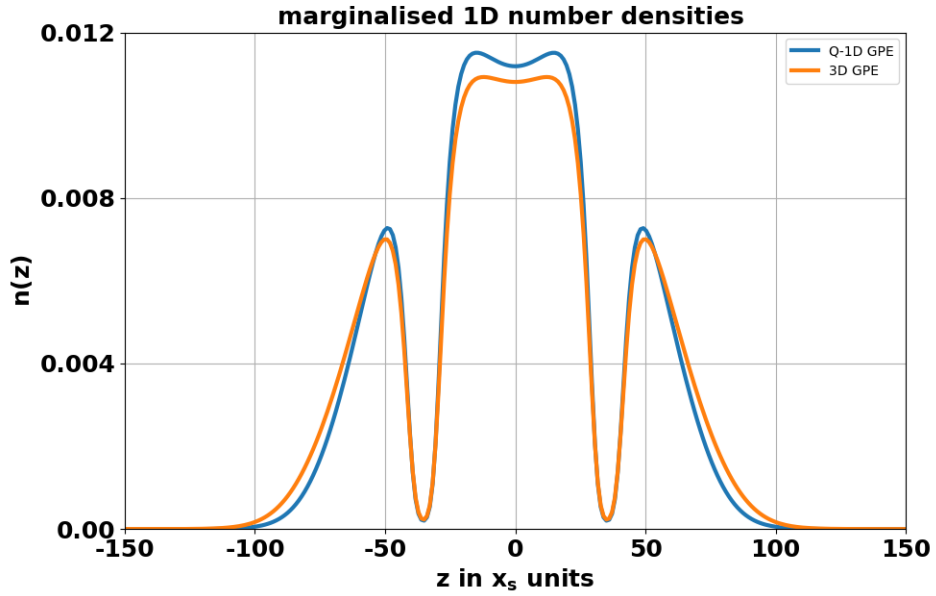

Figure 4.8: Plot for Disc Integrated number density of $n_3^{disc}(z)$ vs its corresponding Q-1D solution. With system paramters $\delta = 6x_s$, $\gamma = 3$, $\xi = 35x_s$, $\tilde{g} = 215$ and $\tilde{g}_d = 51$ this is same case as figure 4.4.

1. Figure 4.8: Exactly same case as figure 4.4. One can see that we have a decent match. In all simulations, one get qualitatively same solution, using Q-1D or 3D. The value of $\mu^{1D} = -0.002837$ and for 3D it was $\mu = 0.998102$. $1 + \mu^{1D} = 0.997163$, similar to μ. This is as expected from a decent Q-1D approximation.

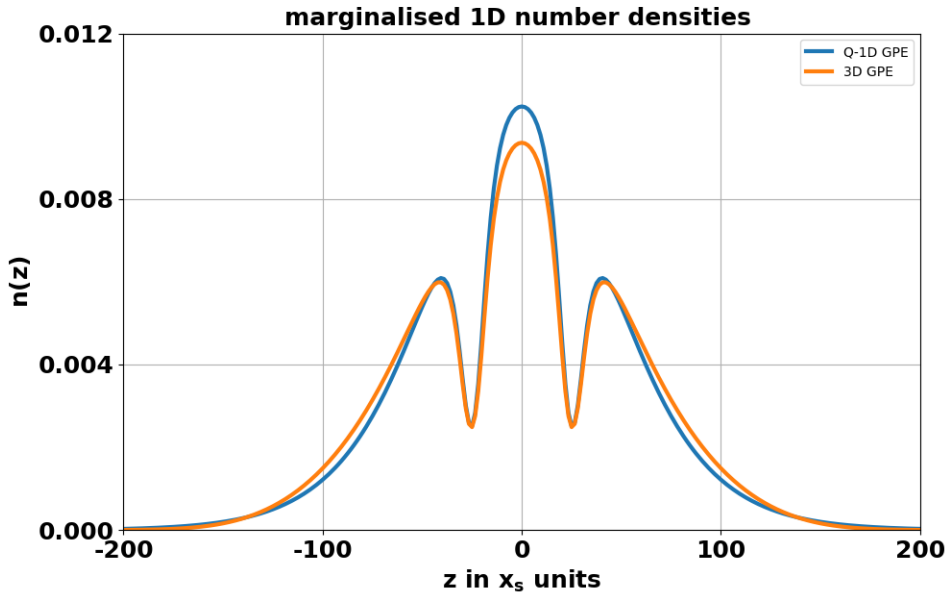

Figure 4.9: Plot for Disc Integrated number density of $n_3^{disc}(z)$ vs its corresponding Q-1D solution. With system paramters $\delta = 6x_s$, $\gamma = 3$, $\xi = 25x_s$, $\tilde{g} = 21$ and $\tilde{g}_d = 5$ this is same case as figure 4.5.

2. Figure 4.9:Exactly same case as figure 4.5. One can see that again we have a decent match even with very different dipolar and contact term. The value of $\mu^{1D} = -0.000182$ and for 3D it was $\mu = 0.999892$. $1 + \mu^{1D} = 0.999818$, again close to μ.

It is worth noting that along with similar values of chemical potential, we have very good match up in integrated density profiles. Even in 3D we observed cylindrical symmetry. The interaction terms were of the order of 10^0 to 10^2. So, the radial direction is a perturbed simple harmonic oscillator (SHO) ground state solution 1.4.2. The contribution to the chemical potential from radial direction in lowest order of approximation is thus 1 in $\hbar\omega_\perp$ units. Certainly, perturbations to this energy scale will highly dominate our energy scales responsible for confinement, which are of order less than 10^{-1}.

4.4 Creating a Periodic Lattice

This scheme of inducing confinement and density modulations via inter-layer dipolar effects has a very straight forward extension. The idea is conveyed in figure 4.10. As can be seen here, the ground state of condensate in lower layer is almost periodically modulated. We present some other examples of control here.

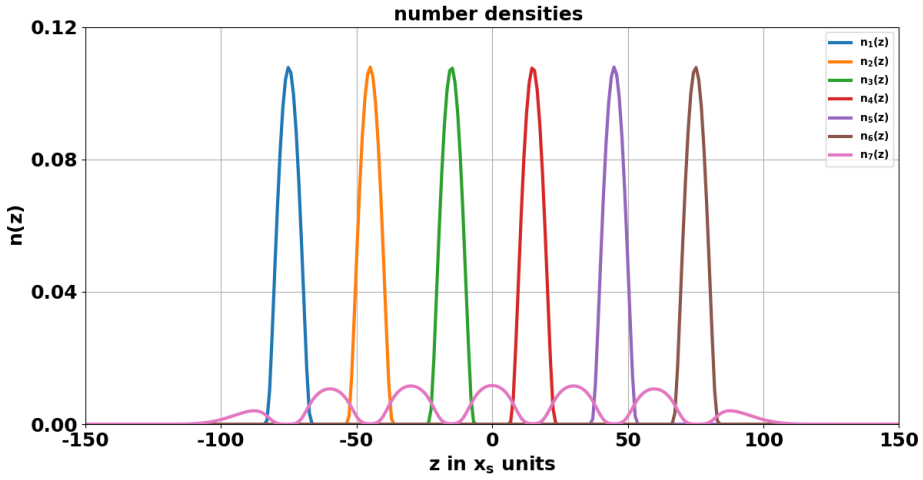

Figure 4.10: Here we have six condensates in upper layer (from n_1 to n_6) and not just two (as was in figure 3.1). With system parameters $\delta = 6x_s$, $\gamma = 3$, $\tilde{g} = 424$ and $\tilde{g}_d = 101$. Traps in upper layer are all separated by a distance of $30x_s$.

1. Figure 4.11 is a 3D ground state result from simulating with six condensate equi-separated in upper layer. Here we have separation between traps as $30x_s$. We saw in our previous simulations that this tends to give sharp peaks in center - like in figure 4.7, where separation was $34x_s$.

2. Figure 4.12 has separation between traps as $50x_s$. Everything else is same as in (1). Simple manipulations in upper layer have created very non-trivial but controllable matter wave without any external optical lattice.

3. Figure 4.13 has separation between traps as $50x_s$. Everything is same as in (2) only number of bosons is different. Changing number of bosons by five to ten times creates drastic qualitative differences here (compare with figure 4.12).

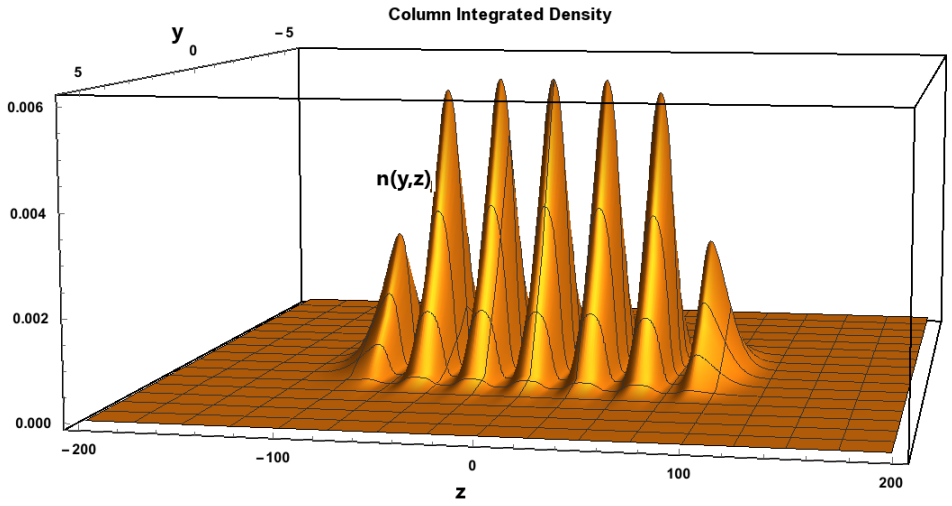

Figure 4.11: Here we have a 3D simulation result of a configuration just like figure 4.10. Only lower layer condensate's number density is being plotted. With system parameters $\delta = 6x_s$, $\gamma = 3$, $\tilde{g} = 215$ and $\tilde{g}_d = 51$, trap separation is again $30x_s$.

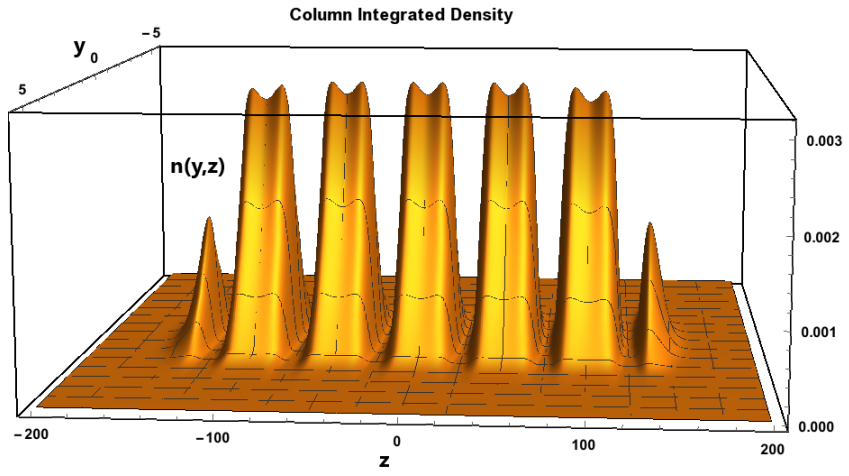

Figure 4.12: This is same as (1). Only trap separation is changed to $50x_s$. Increasing separation between condensates of upper layer creates the dips over the bigger lobes.

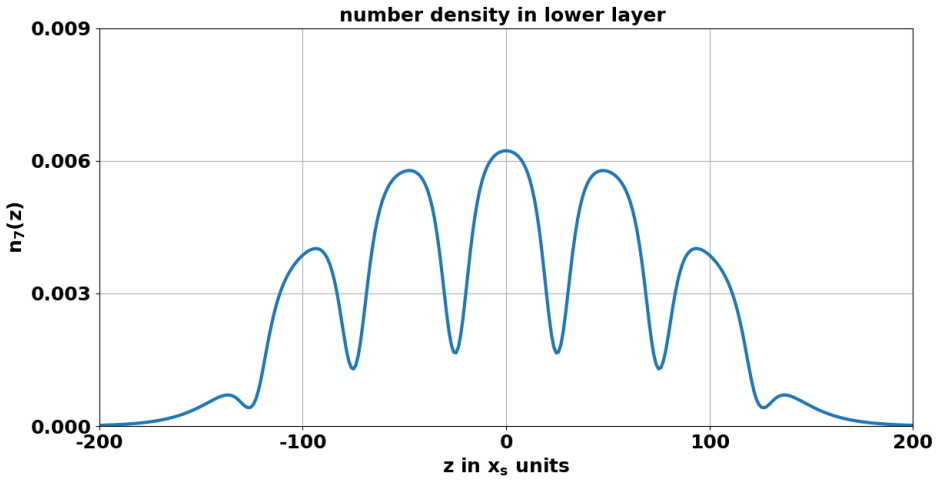

Figure 4.13: Here we have changed the number of bosons. So, system parameters are $\delta = 6x_s$, $\gamma = 3$, $\tilde{g} = 21$ and $\tilde{g}_d = 5$, trap separation is $50x_s$. Just like in the original system 3.1 for the case of lesser number of bosons as in 4.5, condensate's dip was shallow. This is an $x - y$ integrated density profile of a full 3D solution.

4.5 Control over Density and Coherence

In section 4.3.1 we presented four figures with varying parameters, either N - the number of bosons, or ξ - position of traps. From comparing figure 4.4 to figure 4.5, we notice that the density minima is significantly affected with from N. In between figure 4.6, figure 4.7 and figure 4.4 we notice significant change in density profile at the central lobe. This is simply due to variation in ξ, illuminating the degree of customizability of our technique. The ratio between 1^{st} minima and central maxima in such cases is presented in figure 4.14 for a fixed configuration, albeit varying g and g_d in proportion by changing N.

The vanishing ratio hints towards robustness of coherence between the density peaks. For that we quantify coherence between the lobes based on Josephson tunneling [6]. We define a symmetric hopping term E_j and an onsite term E_c for the side peaks.

$$E_J = \int d^3r \phi_1 \left(-\frac{\hbar^2 \nabla^2}{2m} + \int d^3r' V_{dd} (|\psi_1'|^2 + |\psi_2'|^2) \right) \phi_2 \tag{4.6}$$

$$E_c = \int \left[\frac{g}{2} |\phi_1|^4 + |\phi_1|^2 \int d^3r' V_{dd} \, |\phi_1'|^2 \right] \mathrm{d}^3\mathbf{r} \tag{4.7}$$

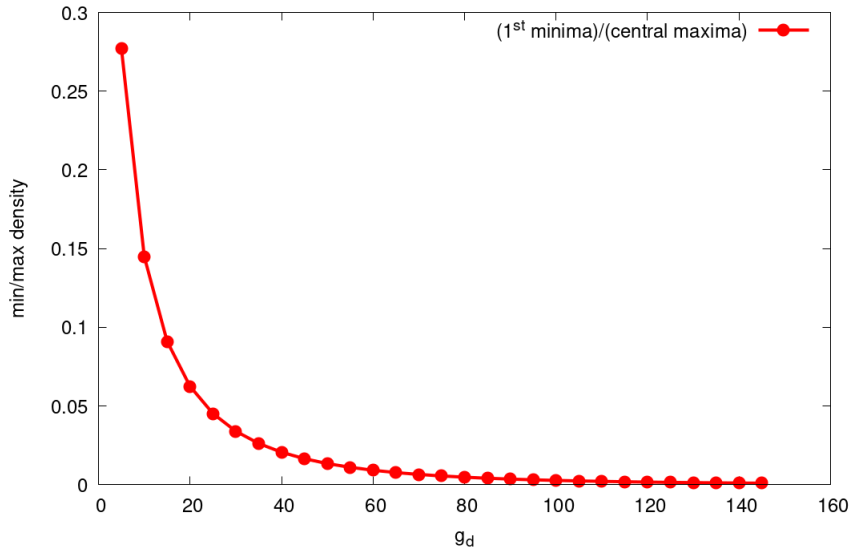

Figure 4.14: Plot for ratio of first minimum versus central maximum for two trapped condensates in upper layer case. With system parameters $\delta = 6x_s$, $\gamma = 3$ and $\xi = 35x_s$ with ratio of $\tilde{g}^{1D}$ and $\tilde{g}_d^{1D}$ kept same as 215/51, i.e. stable regime.

where, ϕ_1 and ϕ_2 are the unit normalised densities of the side peak and the central peak respectively. In our calculations we consider the peaks such that we get a reasonable lower bound on E_j/E_c.

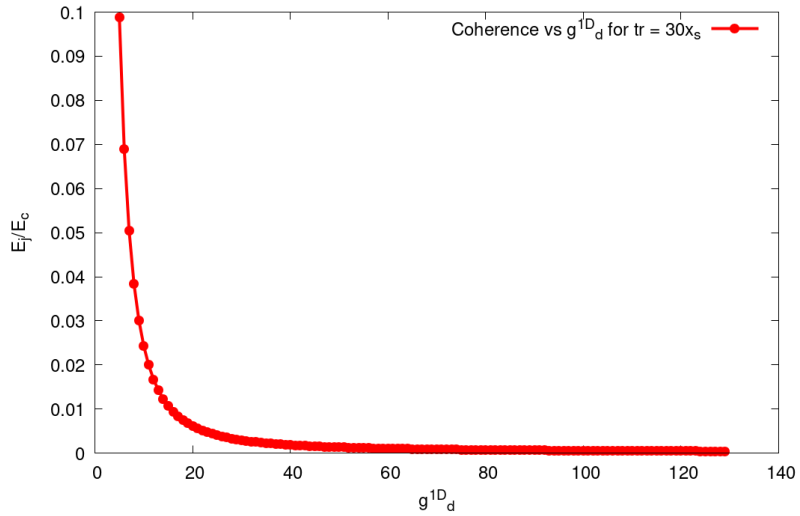

Figure 4.15: Plot for E_j/E_c with system parameters $\delta = 6x_s$, $\gamma = 3$ and $tr = \xi = 30x_s$ with ratio of $\tilde{g}^{1D}$ and $\tilde{g}_d^{1D}$ kept same as in figure 4.14. Gives an estimate of hopping tendency of bosons from side peak to center.

Also, if we are to change the trap position, ξ (tr), we get the following figure 4.16 for the Josephson tunneling from side peak to center.

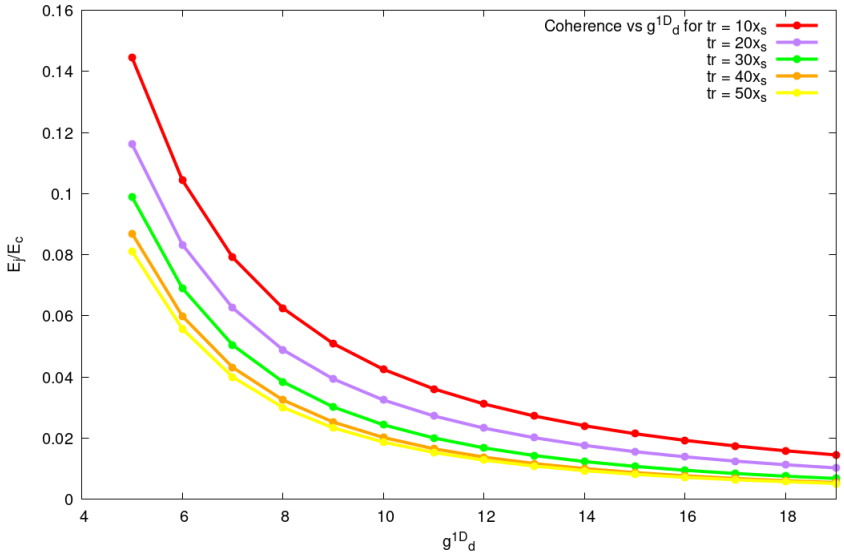

Figure 4.16: Plot for E_j/E_c with system parameters $\delta = 6x_s$, $\gamma = 3$ and $tr = \xi$ from $10x_s$ to $50x_s$ with ratio of $\tilde{g}^{1D}$ and $\tilde{g}_d^{1D}$ kept same as in figure 4.14.

This value of E_j/E_c as we have calculated signifies the robustness of coherence, the peaks have in between. The tunneling of bosons from side peak to central peak is the channel of superfluid flow which maintains the coherence of the whole condensate. This value also signifies the tolerance of the superfluid channel and the coherence between the lobes against dissipative effects of quantum and thermal fluctuations [6].

4.6 Supersolids

We have talked about going beyond the *mean field regime* and droplets and some other non-trivial structures in system at the beginning of this chapter. We also mentioned this is achieved by a precise balance between the parameters and ramping them high enough to reach a regime where our mean-field treatment breaks down and Quantum Fluctuations take over [5]. For dipolar condensates, like we have - prolate cigar shaped trap with dipoles head to tail, one has to control the parameters $\tilde{g}$ and $\tilde{g}_d$ ever so precisely that they tend to *cancel* each other out. Then one ramps up the number of Bosons N, where Q-1D equations

are not valid anymore and the dipolar attraction along the radial direction overcomes the geometric stabilisation of the radial traps and condensate collapses. At least this is what mean-field predicts. However, now that there is high number density and other interactions effectively balance each other out, thus Quantum Fluctuation becomes more prominent. This balance leads to formation of droplets in oblate traps. However ground state is a single droplet and the arrays are high entropy states and thus incoherent [48]. There has to be some superfluid flow between the droplets to maintain coherence. In mean-field solutions, if the lobes/droplets are connected by a channel of superfluid background, coherence exists. In terms of GPE simulations, if the condensate density between droplets is not very low, we have superfluid flow, as well as crystal structure in the matter wave. This is the sought-after supersolid state of matter. Some important work in this direction that I am presently aware of are [61–65].

4.7 Summary and Implications

We have found that we can induced density modulations which can be extended to form a lattice as in figure 4.13 and figure 4.10. These density modulations can have qualitative and quantitative variations depending on parameters effecting the interlayer interactions (see 4.3.1). Also right in the previous sections we quantitatively established the control over bosons hopping from central peak to side lobes by changing N - Boson number. Both these points lead us to the fact that we have attained a state of quantum matter which is a very close imitation of the supersolid state of matter - as we had proposed. The periodic modulations in the ground state of the system is not self-organised, as the condensates in upper layer are externally held. Hence, we don't have a supersolid in conventional sense of the term. Even then, we have achieved inter-layer induced density modulations with coherent flow - effectively what is expected of the sought-after supersolid state of matter. In the mean field regime, we have found a way to induce entrapment and density modulations without aid of any optical trap configuration. Further, the avenue of control offered by the inter-layer effects on changing the properties of the matter wave is of immense importance in the age on Quantum Technologies. We hope this new method to trap with only transverse lasers opens new avenues in experiments and motivate structural engineering of matter wave thus en-route to Quantum Technology applications.

Appendix A

All you need to Simulate a GPE

A near perfect tool to deal with Non-Linear Schrodinger Equation (NLSE), is the Split Operator method.

$$i\hbar\frac{\partial\Psi(\mathbf{r},t)}{\partial t} = \left[-\frac{\hbar^2}{2m}\nabla^2 + V(\mathbf{r}) + g|\Psi(\mathbf{r},t)|^2\right]\Psi(\mathbf{r},t), \tag{A.1}$$

It is basically a pseudo-spectral differential equation solver. Pseudo in the sense that we break Hamiltonian into parts and solve the Laplacian part in momentum space. To do that, we use Forward and Inverse Fourier Transforms. Represent the momentum operator by $\hat{k}$. Consider the position space component to be comprised of $\hat{H}_r = [V(\mathbf{r}) + g|\Psi(\mathbf{r},t)|^2]\,\Psi(\mathbf{r},t)$ and momentum space part as $\hat{H}_k = \left[-\frac{\hbar^2}{2m}\nabla^2\right]\Psi(\mathbf{r},t)$.
For a time-independent Hamiltonian, we have exact time evolution given by:

$$\Psi(\mathbf{r},t+dt) = \left[e^{-\frac{i\hat{H}dt}{\hbar}}\right]\Psi(\mathbf{r},t) = \left[e^{-\frac{i(\hat{H}_r+\hat{H}_k)dt}{\hbar}}\right]\Psi(\mathbf{r},t) \tag{A.2}$$

Here we use the Baker-Campbell-Housdorff formula. With a time-step dt, for $O(dt^2)$ accuracy, using BCH formula gives us

$$\Psi(\mathbf{r},t+dt) = \left[e^{-\frac{i\hat{H}_r dt}{\hbar}}e^{-\frac{i\hat{H}_k dt}{\hbar}}e^{-\frac{[i\hat{H}_r,i\hat{H}_k]dt^2}{2}}\right]\Psi(\mathbf{r},t) \tag{A.3}$$

Ignoring all commutators, we incur an $O(dt^2)$ error. We can get a better approximation

by using Strang Split method:

$$\Psi(\mathbf{r}, t+dt) = \left[e^{-\frac{i\hat{H}_r dt}{2\hbar}} e^{-\frac{i\hat{H}_k dt}{\hbar}} e^{-\frac{i\hat{H}_r dt}{2\hbar}} \right] \Psi(\mathbf{r}, t) + \mathcal{O}(dt^3) \tag{A.4}$$

This will have an additional cost in terms of computation steps but the accuracy outweighs time consumption in most cases.
We now choose to avoid the expensive Laplacian calculation by doing it in the momentum space as follows:

$$\Psi(\nabla, t+dt) = \left[\hat{U}_r \left(\frac{dt}{2} \right) \mathcal{F}^{-1} \left[\hat{U}_k(dt) \mathcal{F} \left[\hat{U}_r \left(\frac{dt}{2} \right) \Psi(\mathbf{r}, t) \right] \right] \right] + \mathcal{O}(dt^3) \tag{A.5}$$

where $\hat{U}_r = e^{-\frac{i\hat{H}_r dt}{\hbar}}$, $\hat{U}_k = e^{-\frac{i\hat{H}_k dt}{\hbar}}$ and $\mathcal{F}$ and $\mathcal{F}^{-1}$ are Forward and Inverse Fourier Transforms. Repeat till equilibrium and Viola! We're done.[1]

[1] Go to https://www.algorithm-archive.org for a nice discussion.

Appendix B

Dimension Reduction Procedure

Here we describe how to reduce Dimension of a 3D GPE to Q-1D. A nice approach to numerical techniques and and mathematical treatment to approximations in GPEs can be found in [15]

Lets look at the Energy equation with only Simple Harmonic trap and contact forces.

$$E(\psi) = \int_{\mathbb{R}^3} \left[\frac{\hbar^2}{2m} |\nabla \psi(\mathbf{x}, t)|^2 + V(\mathbf{x}) |\psi(\mathbf{x}, t)|^2 + \frac{Ng}{2} |\psi(\mathbf{x}, t)|^4 \right] d\mathbf{x} \tag{B.1}$$

The 3-D Gross-Pitaevskii equation is given as

$$\iota\hbar\partial_t\psi = \frac{\delta E(\psi)}{\delta\overline{\psi}} = \left[-\frac{\hbar^2}{2m}\nabla^2 + V(\mathrm{x}) + Ng|\psi|^2 \right] \psi, \quad \mathrm{x} \in \mathbb{R}^3, \quad t > 0 \tag{B.2}$$

The trapping potential is Simple Harmonic. i.e.

$$V(\mathrm{x}) = \frac{m}{2} \left(\omega_x^2 x^2 + \omega_y^2 y^2 + \omega_z^2 z^2 \right), \quad \mathrm{x} = (x, y, z)^T \in \mathbb{R}^3 \tag{B.3}$$

WLOG, we would be considering $\omega_x \geq \omega_y \geq \omega_z$.

From the GPE [B.2] we get the non-dimensional equation given below. The scaling is done with respect to $t_s = \frac{1}{\omega_x}, x_s = \sqrt{\frac{\hbar}{m\omega_x}}$ and $E_s = \hbar\omega_x$. Also the normalisation needs to be taken care of.

$$i\partial_t\psi(\mathrm{x}, t) = \left[-\frac{1}{2}\nabla^2 + V(\mathrm{x}) + \kappa|\psi(\mathrm{x}, t)|^2 \right] \psi(\mathrm{x}, t), \quad \mathrm{x} \in \mathbb{R}^3, \quad t > 0 \tag{B.4}$$

where $\kappa = \frac{4\pi N a_s}{x_s}$ (a_s is the s-wave scattering length) and the non-dimensional trap is given as:

$$V(\mathrm{x}) = \frac{1}{2}\left(x^2 + \gamma_y^2 y^2 + \gamma_z^2 z^2\right), \quad \mathrm{x} \in \mathbb{R}^3, \quad \text{with } \gamma_y = \frac{\omega_y}{\omega_x} \geq 1, \gamma_z = \frac{\omega_z}{\omega_x} \geq 1 \tag{B.5}$$

When Anisotropy is high enough, i.e. $\gamma_y >> 1$and/or $\gamma_z >> 1$, we can reduce the 3D equation [B.4] to a 2-D or 1-D equation in the weak interaction regime($1/\kappa = O(\gamma_y)$) at least.
In this regime the most significant part of the Hamiltonian is same as that of the Simple Harmonic Oscillator in the y and z and some other terms for the x direction. The y and z part can be assumed to be in ground state and thus the solution for the 3-D equation [B.4] factors approximately as

$$\psi(\mathrm{x}, t) \approx \psi_2(x, t)\, \omega_0(y, z) e^{-i\mu_0^{\gamma} t}, \quad x \in \mathbb{R}, \quad t \geq 0 \tag{B.6}$$

where ω_0 is a gaussian.
We put this in 3-D GPE [B.4] and then after some manipulation multiply the LHS and RHS with $\omega_0(y, z)$ and integrate over y and z to obtain the following.

$$i\partial_t \psi(x, t) = \left[-\frac{1}{2}\partial_{xx} + \frac{x^2}{2} + \kappa \frac{\sqrt{\gamma_y \gamma_z}}{2\pi} |\psi(x, t)|^2\right] \psi(x, t), \quad x \in \mathbb{R}, \quad t > 0 \tag{B.7}$$

The gamma factors come after the integration.

The dipolar term in the GP equation [B.2] is given as

$$\int d\mathbf{r}' V_d(\mathbf{r} - \mathbf{r}') |\Psi(\mathbf{r}')|^2$$

where $V_d(\mathbf{r} - \mathbf{r}') = g_d N (1 - 3\cos^2\theta) / |\mathbf{r} - \mathbf{r}'|^3$.
Using forward and inverse Fourier Transforms on this term we get,

$$\int d\mathbf{r}' V_d(\mathbf{r} - \mathbf{r}') |\Psi(\mathbf{r}')|^2 = (2\pi)^3 \int \hat{V}_d(\mathbf{k}) \hat{n}(\mathbf{k}) e^{-\iota \mathbf{k}\cdot\mathbf{r}} d\mathbf{k} \tag{B.8}$$

where $\hat{V}_d(\mathbf{k})$ = C [$3k_x^2/|\mathbf{k}|^2$ -1] for all dipoles oriented in the X direction. Now, since $\psi(\mathbf{x}, t)$ could be factored, we factor $\hat{n}(\mathbf{k})$ as $\hat{n}_x(k_x)|\hat{\omega}(k_y, k_z)|^2$. If the process of Dimension reduction is followed, we would essentially be integrating the dipolar term $(2\pi)^3 \int \hat{V}_d(\mathbf{k}) \hat{n}(\mathbf{k}) e^{-\iota \mathbf{k}\cdot\mathbf{r}} d\mathbf{k} |\Psi(\mathbf{r})|$ (all factored up) multiplied by $|\omega_0(y, z)|^2$ over y and z.

Bibliography

[1] R Feynman. There's plenty of room at the bottom, engineering and science. *California: California Institute Of Technology*, 1960.

[2] T Lahaye, C Menotti, L Santos, M Lewenstein, and T Pfau. The physics of dipolar bosonic quantum gases. *Reports on Progress in Physics*, 72(12):126401, nov 2009.

[3] M.A. Baranov. Theoretical progress in many-body physics with ultracold dipolar gases. *Physics Reports*, 464(3):71–111, 2008.

[4] Lauriane Chomaz, Rick Bijnen, Daniel Petter, Giulia Faraoni, Simon Baier, Jan Becher, Manfred Mark, Falk Waechtler, Luis Santos, and Francesca Ferlaino. Observation of the roton mode in a dipolar quantum gas. *Nature Physics*, 14, 05 2018.

[5] D. Baillie and P. B. Blakie. Droplet crystal ground states of a dipolar bose gas. *Phys. Rev. Lett.*, 121:195301, Nov 2018.

[6] Matthias Wenzel, Fabian Böttcher, Tim Langen, Igor Ferrier-Barbut, and Tilman Pfau. Striped states in a many-body system of tilted dipoles. *Physical Review A*, 96(5):053630, 2017.

[7] Thorsten Köhler, Krzysztof Góral, and Paul S. Julienne. Production of cold molecules via magnetically tunable feshbach resonances. *Rev. Mod. Phys.*, 78:1311–1361, Dec 2006.

[8] The nobel prize in physics 1913. *NobelPrize.org.*

[9] K. B. Davis, M. O. Mewes, M. R. Andrews, N. J. van Druten, D. S. Durfee, D. M. Kurn, and W. Ketterle. Bose-einstein condensation in a gas of sodium atoms. *Phys. Rev. Lett.*, 75:3969–3973, Nov 1995.

[10] Masahito Ueda. *Fundamentals and new frontiers of Bose-Einstein condensation*. World Scientific, 2010.

[11] Lev Pitaevskii and Sandro Stringari. *Bose-Einstein condensation and superfluidity*, volume 164. Oxford University Press, 2016.

[12] Carlo F Barenghi and Nick G Parker. *A primer on quantum fluids*. Number arXiv: 1605.09580. Springer, 2016.

[13] T. D. Lee and C. N. Yang. Many-body problem in quantum mechanics and quantum statistical mechanics. *Phys. Rev.*, 105:1119–1120, Feb 1957.

[14] Elliott H. Lieb and Robert Seiringer. Proof of bose-einstein condensation for dilute trapped gases. *Phys. Rev. Lett.*, 88:170409, Apr 2002.

[15] Weizhu Bao, Dieter Jaksch, and Peter A Markowich. Numerical solution of the gross–pitaevskii equation for bose–einstein condensation. *Journal of Computational Physics*, 187(1):318–342, 2003.

[16] Thierry Dauxois and Michel Peyrard. *Physics of solitons*. Cambridge University Press, 2006.

[17] Philip G Drazin and Robin S Johnson. *Solitons: an introduction*, volume 2. Cambridge university press, 1989.

[18] DJ Frantzeskakis. Dark solitons in atomic bose–einstein condensates: from theory to experiments. *Journal of Physics A: Mathematical and Theoretical*, 43(21):213001, 2010.

[19] Stefan Burger, Kai Bongs, Stefanie Dettmer, Wolfgang Ertmer, Klaus Sengstock, Anna Sanpera, Gora V Shlyapnikov, and Maciej Lewenstein. Dark solitons in bose-einstein condensates. *Physical Review Letters*, 83(25):5198, 1999.

[20] J Denschlag, Je E Simsarian, Dl L Feder, Charles W Clark, La A Collins, J Cubizolles, Lu Deng, Edward W Hagley, Kristian Helmerson, William P Reinhardt, et al. Generating solitons by phase engineering of a bose-einstein condensate. *Science*, 287(5450):97–101, 2000.

[21] Christoph Becker, Simon Stellmer, Parvis Soltan-Panahi, Sören Dörscher, Mathis Baumert, Eva-Maria Richter, Jochen Kronjäger, Kai Bongs, and Klaus Sengstock. Os-

cillations and interactions of dark and dark–bright solitons in bose–einstein condensates. *Nature Physics*, 4(6):496–501, 2008.

[22] Joachim Brand and William P Reinhardt. Solitonic vortices and the fundamental modes of the "snake instability": Possibility of observation in the gaseous bose-einstein condensate. *Physical Review A*, 65(4):043612, 2002.

[23] Gunjan Verma, Umakant D Rapol, and Rejish Nath. Generation of dark solitons and their instability dynamics in two-dimensional condensates. *Physical Review A*, 95(4):043618, 2017.

[24] TP Billam, AL Marchant, SL Cornish, SA Gardiner, and NG Parker. Bright solitary matter waves: formation, stability and interactions. In *Spontaneous Symmetry Breaking, Self-Trapping, and Josephson Oscillations*, pages 403–455. Springer, 2012.

[25] Kevin E Strecker, Guthrie B Partridge, Andrew G Truscott, and Randall G Hulet. Formation and propagation of matter-wave soliton trains. *Nature*, 417(6885):150–153, 2002.

[26] L Khaykovich, F Schreck, G Ferrari, Thomas Bourdel, Julien Cubizolles, Lincoln D Carr, Yvan Castin, and Christophe Salomon. Formation of a matter-wave bright soliton. *Science*, 296(5571):1290–1293, 2002.

[27] Jason HV Nguyen, Paul Dyke, De Luo, Boris A Malomed, and Randall G Hulet. Collisions of matter-wave solitons. *Nature Physics*, 10(12):918–922, 2014.

[28] AL Marchant, TP Billam, TP Wiles, MMH Yu, SA Gardiner, and SL Cornish. Controlled formation and reflection of a bright solitary matter-wave. *Nature communications*, 4(1):1–6, 2013.

[29] Axel Griesmaier, Jörg Werner, Sven Hensler, Jürgen Stuhler, and Tilman Pfau. Bose-einstein condensation of chromium. *Phys. Rev. Lett.*, 94:160401, Apr 2005.

[30] John Doyle, Bretislav Friedrich, RV Krems, and Françoise Masnou-Seeuws. Quo vadis, cold molecules?, 2004.

[31] Silke Ospelkaus, A Pe'Er, K-K Ni, JJ Zirbel, B Neyenhuis, S Kotochigova, PS Julienne, J Ye, and DS Jin. Efficient state transfer in an ultracold dense gas of heteronuclear molecules. *Nature Physics*, 4(8):622–626, 2008.

[32] K-K Ni, S Ospelkaus, MHG De Miranda, A Pe'Er, B Neyenhuis, JJ Zirbel, S Kotochigova, PS Julienne, DS Jin, and Jun Ye. A high phase-space-density gas of polar molecules. *science*, 322(5899):231–235, 2008.

[33] J. Deiglmayr, A. Grochola, M. Repp, K. Mörtlbauer, C. Glück, J. Lange, O. Dulieu, R. Wester, and M. Weidemüller. Formation of ultracold polar molecules in the rovibrational ground state. *Phys. Rev. Lett.*, 101:133004, Sep 2008.

[34] Chinmayee Mishra, Luis Santos, and Rejish Nath. Self-bound doubly dipolar bose-einstein condensates. *Physical review letters*, 124(7):073402, 2020.

[35] Mark Saffman, Thad G Walker, and Klaus Mølmer. Quantum information with rydberg atoms. *Reviews of modern physics*, 82(3):2313, 2010.

[36] N Bogoliubov. On the theory of superfluidity. *J. Phys*, 11(1):23, 1947.

[37] Thierry Lahaye, Jonas Metz, Bernd Froehlich, Tobias Koch, Maximilian Meister, Axel Griesmaier, Tilman Pfau, Hiroki Saito, Yuki Kawaguchi, and Masahito Ueda. d-wave collapse and explosion of a dipolar bose-einstein condensate. *Physical review letters*, 101(8):080401, 2008.

[38] L. Santos, G. V. Shlyapnikov, and M. Lewenstein. Roton-maxon spectrum and stability of trapped dipolar bose-einstein condensates. *Phys. Rev. Lett.*, 90:250403, Jun 2003.

[39] T. D. Lee, Kerson Huang, and C. N. Yang. Eigenvalues and eigenfunctions of a bose system of hard spheres and its low-temperature properties. *Phys. Rev.*, 106:1135–1145, Jun 1957.

[40] L. Santos, G. V. Shlyapnikov, and M. Lewenstein. Roton-maxon spectrum and stability of trapped dipolar bose-einstein condensates. *Phys. Rev. Lett.*, 90:250403, Jun 2003.

[41] D. Guéry-Odelin and S. Stringari. Scissors mode and superfluidity of a trapped bose-einstein condensed gas. *Phys. Rev. Lett.*, 83:4452–4455, Nov 1999.

[42] O. M. Maragò, S. A. Hopkins, J. Arlt, E. Hodby, G. Hechenblaikner, and C. J. Foot. Observation of the scissors mode and evidence for superfluidity of a trapped bose-einstein condensed gas. *Phys. Rev. Lett.*, 84:2056–2059, Mar 2000.

[43] F. S. Cataliotti, S. Burger, C. Fort, P. Maddaloni, F. Minardi, A. Trombettoni, A. Smerzi, and M. Inguscio. Josephson junction arrays with bose-einstein condensates. *Science*, 293(5531):843–846, 2001.

[44] Krzysztof Góral, Kazimierz Rzążewski, and Tilman Pfau. Bose-einstein condensation with magnetic dipole-dipole forces. *Phys. Rev. A*, 61:051601, Mar 2000.

[45] L. Santos, G. V. Shlyapnikov, P. Zoller, and M. Lewenstein. Bose-einstein condensation in trapped dipolar gases. *Phys. Rev. Lett.*, 85:1791–1794, Aug 2000.

[46] S. Yi and L. You. Trapped condensates of atoms with dipole interactions. *Phys. Rev. A*, 63:053607, Apr 2001.

[47] S. Yi and H. Pu. Vortex structures in dipolar condensates. *Phys. Rev. A*, 73:061602, Jun 2006.

[48] Holger Kadau, Matthias Schmitt, Matthias Wenzel, Clarissa Wink, Thomas Maier, Igor Ferrier-Barbut, and Tilman Pfau. Observing the rosensweig instability of a quantum ferrofluid. *Nature*, 530, 08 2015.

[49] Hiroki Saito, Yuki Kawaguchi, and Masahito Ueda. Ferrofluidity in a two-component dipolar bose-einstein condensate. *Phys. Rev. Lett.*, 102:230403, Jun 2009.

[50] G Guijarro, GE Astrakharchik, and J Boronat. Ultradilute quantum liquid of dipolar atoms in a bilayer. *arXiv preprint arXiv:2105.13241*, 2021.

[51] Daw-Wei Wang, Mikhail D. Lukin, and Eugene Demler. Quantum fluids of self-assembled chains of polar molecules. *Phys. Rev. Lett.*, 97:180413, Nov 2006.

[52] S. Müller, J. Billy, E. A. L. Henn, H. Kadau, A. Griesmaier, M. Jona-Lasinio, L. Santos, and T. Pfau. Stability of a dipolar bose-einstein condensate in a one-dimensional lattice. *Phys. Rev. A*, 84:053601, Nov 2011.

[53] R. Nath, P. Pedri, and L. Santos. Soliton-soliton scattering in dipolar bose-einstein condensates. *Phys. Rev. A*, 76:013606, Jul 2007.

[54] Kazimierz Łakomy, Rejish Nath, and Luis Santos. Soliton molecules in dipolar bose-einstein condensates. *Phys. Rev. A*, 86:013610, Jul 2012.

[55] Matthias Rosenkranz, Yongyong Cai, and Weizhu Bao. Effective dipole-dipole interactions in multilayered dipolar bose-einstein condensates. *Phys. Rev. A*, 88:013616, Jul 2013.

[56] Chao-Chun Huang and Wen-Chin Wu. Center motions of nonoverlapping condensates coupled by long-range dipolar interaction in bilayer and multilayer stacks. *Phys. Rev. A*, 82:053612, Nov 2010.

[57] Daw-Wei Wang and Eugene Demler. Collective excitations and instabilities in multilayer stacks of dipolar condensates. *arXiv preprint arXiv:0812.1838*, 2008.

[58] Matthias Rosenkranz, Yongyong Cai, and Weizhu Bao. Effective dipole-dipole interactions in multilayered dipolar bose-einstein condensates. *Physical Review A*, 88(1):013616, 2013.

[59] William D Phillips. Nobel lecture: Laser cooling and trapping of neutral atoms. *Reviews of Modern Physics*, 70(3):721, 1998.

[60] David J Wineland, Jean Dalibard, and C Cohen-Tannoudji. Sisyphus cooling of a bound atom. *JOSA B*, 9(1):32–42, 1992.

[61] Santo Maria Roccuzzo and Francesco Ancilotto. Supersolid behavior of a dipolar bose-einstein condensate confined in a tube. *Phys. Rev. A*, 99:041601, Apr 2019.

[62] Yves Pomeau and Sergio Rica. Dynamics of a model of supersolid. *Phys. Rev. Lett.*, 72:2426–2429, Apr 1994.

[63] Fabian Böttcher, Jan-Niklas Schmidt, Matthias Wenzel, Jens Hertkorn, Mingyang Guo, Tim Langen, and Tilman Pfau. Transient supersolid properties in an array of dipolar quantum droplets. *Phys. Rev. X*, 9:011051, Mar 2019.

[64] Matthias Wenzel, Fabian Böttcher, Tim Langen, Igor Ferrier-Barbut, and Tilman Pfau. Striped states in a many-body system of tilted dipoles. *Phys. Rev. A*, 96:053630, Nov 2017.

[65] Massimo Boninsegni and Nikolay V. Prokof'ev. Colloquium: Supersolids: What and where are they? *Rev. Mod. Phys.*, 84:759–776, May 2012.